Knapp, Blayne A., Water Deprivation Evokes Changes in Glutamate Neurotransmission in Magnocellular Neurosecretory Cells of the Hypothalamic Supraoptic Nucleus. Master of Science in Integrative Physiological Research, April 2015, 60 pp., 2 tables, 16 figures, appendix, bibliography 71 references.

The regulation of vasopressin (AVP) is critical to maintaining body fluid homeostasis, and the activity of magnocellular neurosecretory cells (MNCs) correlates to the amount of hormone secreted into circulation. The balance of excitatory and inhibitory inputs are important elements of activity, however the mechanisms leading to changes in AVP regulation are not fully understood. Water deprivation (WD), a physiological challenge, was used to examine changes in excitatory neurotransmission in MNCs, measured using patch-clamp electrophysiology and ratiometric calcium imaging. An adeno-associated virus construct containing an AVP gene promoter and enhanced green fluorescent protein (EGFP) reporter allowed us to distinguish vasopressin from oxytocin MNCs. In EGFP-labeled cells (GFP+ MNCs), 48-hour WD treatment resulted in significantly greater mini-excitatory postsynaptic current (mEPSC) amplitude as compared to euhydrated animals. GFP+ MNCs exhibited greater calcium mobilization than GFP- MNCs independent of treatment group, and we observed less cytosolic calcium mobilization with 48H WD treatment.

WATER DEPRIVATION EVOKES CHANGES IN GLUTAMATE NEUROTRANMISSION IN MAGNOCELLULAR NEUROSECRETORY CELLS OF THE HYPOTHALAMIC SUPRAOPTIC NUCLEUS

Blayne A. Knapp, B.A.

Approved:

_____
Dr. Tom Cunningham, Major Professor

_____
Dr. Steve Mifflin, Committee Member

_____
Dr. Ann Schreihofer, Committee Member

_____
Dr. Michael Gatch, University Member

_____
Dr. Steve Mifflin, Chair of Integrative Physiology

_____
Dr. Meharvan Singh, Dean, Graduate School of Biomedical Sciences

WATER DEPRIVATION EVOKES CHANGES IN GLUTAMATE NEUROTRANMISSION IN MAGNOCELLULAR NEUROSECRETORY CELLS OF THE HYPOTHALAMIC SUPRAOPTIC NUCLEUS

THESIS

Presented to the Graduate Council of the

Graduate School of Biomedical Sciences

University of North Texas

Health Science Center at Fort Worth

in Partial Fulfillment of the Requirements

For the Degree of

Masters of Science

By

Blayne A Knapp, B.A.

Fort Worth, Texas

April 2015

ACKNOWLEDGEMENTS

I would like to express my deepest appreciation to all those who have been instrumental and supportive in the successful completion of this project. I would like to show my greatest appreciation to my major professor, Dr. Tom Cunningham. I would like to thank my committee members, Dr. Ann Schreihofer, Dr. Steve Mifflin, and Dr. Michael Gatch for not only your time but your help and guidance throughout this project. I would like to thank my fellow lab members and post-doc, Dr Prashant Nedungadi, Joel Little, Martha Bachelor, Dr. Ashwini Saxena, Brent Shell and Katelynn Faulk, whose encouragement and help were vital for the success of this project. This work is supported by R56-HL625690.

TABLE OF CONTENTS

LIST OF TABLES

LIST OF FIGURES

INTRODUCTION

Arginine Vasopressin (AVP) is a neurohypophyseal hormone released from the posterior pituitary by magnocellular neurosecretory cells (MNCs) located within the supraoptic (SON) and paraventricular (PVN) nuclei of the hypothalamus[1,2]. Vasopressin is responsible for the regulation of body fluid homeostasis in its ability to influence blood pressure, plasma osmolality, and blood volume[3,4]. It acts by mediating antidiuresis in response to the loss of body fluids by binding V2 receptors (V2R) in the kidney to stimulate insertion of the aquaporin water channel into the distal collecting duct of the kidney and epithelial sodium channel (ENaC) in the apical membrane of the renal collecting ducts' principal cells[5–7]. This results in the reabsorption of water and sodium, thereby influencing blood volume and plasma osmolality. AVP also acts as a potent vasoconstrictor by binding its V1a receptor in vascular smooth muscle[8,9].

The regulation of vasopressin release is critical for maintaining blood volume and blood pressure, and although the molecular mechanisms of AVP regulation are not fully understood, we do know that it is partially due to the vital balance of synaptic excitatory and inhibitory inputs that determine the linear relationship between plasma osmolality and AVP release[1,10–12]. A portion of this regulation is due to glutamatergic and GABAergic projections to MNCs that originate in osmosensitive regions of the brain lying adjacent to the third ventricle such as the organum vasculosum of the lamina terminalis (OVLT), the subfornical organ (SFO) and the median preoptic nucleus (MnPO)[1,13,14]. Previous studies have shown that glutamatergic inputs play an important role in regulating SON MNC excitability, with presynaptic activity of OVLT

pathways modulating the frequency of excitatory postsynaptic currents (mEPSCs) and firing rate of MNCs in proportion with increased fluid osmolality[12]. The OVLT, SFO, and MnPO all convey osmosensitive information to MNCs and in that effect coordinate physiological responses to changes in plasma osmolality[12–16]. Recently, it has also become clear that glial cells which contain extrasynaptic glutamate transporters also strongly influence SON MNC excitatory neurotransmission in response to various physiological stimuli[17–19]. The activation of glutamatergic and GABAergic projections results in the release of these neurotransmitters into the synaptic cleft. The actions of glutamate are mediated through postsynaptic ionotropic AMPA and NMDA (AMPARs and NMDARs) which are nonspecific cation channels that mediate mEPSCS [12,13,16,20–22]. The actions of GABA are mainly mediated through the postsynaptic ionotropic γ-amino- butyric acid type A ($GABA_{A)}$ receptor which under normal physiological conditions, exhibit an inhibitory effect on MNC neurotransmission by mediating miniature inhibitory postysynaptic currents (mIPSCs) [23–25]. These mediators of neurotransmission have the ability to modify their synaptic strength in response to certain stimuli and have been shown to play critical roles in neuroplasticity[12,26–29]. It is the balance of these influences that determine the pattern and frequency of action potential firing in MNCs, hence the release of vasopressin into circulation. The influence of these pathways and modulators within the milieu of the hypothalamic nuclei have been found to be both osmotically and non-osmotically controlled[1,11,12,22,23,26,29–34].

Currently, there are a number of models being used to elucidate the mechanisms known to alter AVP release in MNCs. Several research groups have reported that physiological stimuli mediate measurable changes in postysynaptic glutamatergic and GABAergic activity in MNCs, but pathways responsible for the changes and the excitatory and inhibitory components

themselves remain controversial[10,24,29,35–37]. The model of water deprivation (WD) used here represents a physiological challenge that requires a sustained release of vasopressin from the posterior pituitary into circulation as a means of maintaining body fluid homeostasis. The importance of using an osmotic stimulus is its ability to evoke a shift to increase the amount of AVP released into circulation, but that the observed changes remain reversible once body fluid homeostasis is restored[1,2,10]. Water deprivation model, when carried out for 24 and 48 hours of dehydration is able to induce significant changes in plasma measurements of arginine vasopressin, plasma osmolality, hematocrit and plasma protein concentrations[38]. These results indicate that, in addition to significant changes in plasma osmolality, water deprivation is associated with significant changes in blood volume and activation of the renin-angiotensin system which could also influence excitatory neurotransmission at the level of the MNCs. This data also showed that rehydration after 24 or 48 hour water deprivation treatment restored the plasma osmolality, circulating vasopressin concentration, hematocrit and plasma protein measurements to control or euhydrated values[38]. Thus, changes in excitatory neurotransmission in MNCs that are associated with water deprivation may also be reversible as opposed to changes in MNC function that may contribute to inappropriate AVP release related to pathophysiological states.

The dysregulation of AVP release observed in disease states such as heart failure, liver cirrhosis and diabetes leads to a sustained and inappropriate release of AVP. This leads to dilutional hyponatremia as patients suffering from these diseases experience increased water retention and diluted electrolytes, resulting in a potentiation of these disease states, further complicating and increasing the expenses of clinical treatment[34–37]. With limited effective treatment options available and increased association of morbidity, patient care becomes

increasingly challenging and expensive. In order to better understand and treat the dysregulation of body fluid homeostasis that occur with these pathologies, the changes in postsynaptic receptor expression and pathways responsible for these changes during physiological stress must be determined.

The model of water deprivation addresses these current challenges, and in recent studies, our labs and others have shown that water deprivation causes reversible changes in postsynaptic NMDA receptor activity in MNCs, thereby enhancing glutamatergic neurotransmission [21,27,28,43–45]. This change in synaptic strength could be important for normal physiological function, and the molecular mechanisms behind these changes in AVP MNCs are still not clearly understood. One model of activity-dependent neuroplasticity that alters both glutamate and GABA neurotransmission, encourage neural growth and the formation of new synapses is the BDNF-TrkB signaling pathway[24,43,46–50]. Brain-derived neurotrophic factor is a member of the nerve growth factor family, and it has previously been shown that BDNF regulates AMPA and NMDA receptor subunit phosphorylation, trafficking and expression through binding its receptor tyrosine kinase B (TrkB)[43,50–55]. BDNF has also been shown to be sensitive to osmotic stress and in the SON, it has previously been shown to be a candidate for mediating changes in glutamate neurotransmission[24,43,50]. Previous work in our lab has determined that water deprivation leads to the phosphorylation of the TrkB receptor, its interaction with Src kinase family member Fyn kinase and the subsequent phosphorylation of the NMDA receptor NR2B subunit[41,48]. NR2B subunit phosphorylation is relevant to glutamate neurotransmission because it has been shown to increase the open time of the NMDA receptor, thereby directly enhancing NMDAR function and contributing to long term potentiation and long term depression in MNCs[43,50,56]. Enhanced NMDAR receptor function is also known to cause increased insertion of AMPARs into the

plasma membrane of MNCs which would further enhance postsynaptic glutamate neurotransmission[58–60].

This study was dedicated to elucidating the functional roles these changes in AMPAR and NMDAR have in AVP MNCs when exposed to WD *in vitro*. The SON of the hypothalamus presents a preferred MNC population to study these effects because of its homogenous population of vasopressin and oxytocin (OXT) MNCs, where the PVN is heterogeneous in expression, containing both MNCs and parvocellular cells. The electrical properties of AVP and OXT MNCs have previously been shown to be distinct from one another, and that the properties of their respective currents are controlled in a cell type-specific manner, which is why differentiating between the two cell types is of primary importance[20]. Oxytocin has been well characterized in its role during lactation and parturition, and in rats, oxytocin has also been characterized as a hormone involved in natriuresis and responsive to stimuli such as hypovolemia, dehydration, and increases in plasma osmolality[1,61–64]. So while oxytocin MNCs are activated in response to water deprivation, the patterns of hormone secretion themselves are different from those observed in vasopressin MNCs. The electrical properties of their response to water deprivation are also characteristically different[12,20,65,66]. Oxytocin MNCs have been shown to be synchronously activated across the whole population, while vasopressin MNCs display several types of activity patterns throughout the whole population, characterized as continuous, phasic, irregular or silent activity[1,13,14,20,63,67]. This is important because with a stimuli such as water deprivation, there is a shift to enhanced amounts phasic and continuous activity observed in AVP MNCs that in the end contribute to the increased release of vasopressin into circulation[29,63]. What is currently unclear is how this shift in AVP MNC activity is carried out, if the changes in AVP MNC excitability are a function of presynaptic inputs, modulation by glia,

or changes in the intrinsic properties of AVP MNCs themselves. In order to visually differentiate AVP MNCs from OXT MNCs, an adeno-associated virus (AAV) construct containing mouse AVP gene promoter and enhanced green fluorescent protein (EGFP) reporter was bilaterally targeted to the SON and used to visualize AVP MNCs within the SON. Through the use of patch-clamp electrophysiology and ratiometric calcium imaging, we were able to address a novel mechanism potentially responsible for changes observed in neurotransmission of MNCs after exposure to water deprivation. Patch-clamp electrophysiology allowed us to measure parameters of mEPSCs, which were used as an assay of glutamatergic neurotransmission. With water deprivation, we expected to observe changes in components of mEPSCs that might explain how this physiological stimulus influences excitatory neurotransmission, therefore we measured mEPSC amplitude, rise time (ms), decay time (ms), charge transfer, and frequency of the mEPSCs. We expected alterations in the phosphorylated NR2B expression in NMDARs to influence the decay time with water deprivation, as well as potential influence on rise time and charge transfer of the mEPSC. With increased AMPAR recruitment to the plasma membrane of MNCs, we expected to observe increases in mEPSC amplitude and charge transfer with water deprivation treatment (Fig. 1). The importance of determining the molecular mechanisms responsible for AVP regulation during health and disease states will bridge current gaps and controversies in our understanding of AVP control and potentially provide novel therapeutic targets to ameliorate AVP dysregulation.

MATERIALS AND METHODS

2.1 Animals

Adult male Sprague-Dawley rats that weighed 250 – 350 g (Charles Rivers, Wilmington, MA, USA) were individually housed and maintained on a 12:12 hour light cycle in a temperature-controlled environment and provided with ad libitum access to food and water except where indicated in specific protocols. All procedures involving animals were conducted according to protocols approved by the Institutional Animal Care and Uses Committee at the University of North Texas Health Science Center, and in accordance with the guidelines of Public Health Service, the American Physiological Society, and the Society for Neuroscience.

2.2 Experimental Protocol

The control group of euhydrated (EU) animals was allowed *ad lib.* access to water and food, whereas the water-deprived animals had no access to water for 24 (24H WD) or 48 (48H WD) hours as noted.

2.3 SON Injections

One week after arrival to the UNT Health Science Center vivarium, rats were anesthetized with 1-5% isofluorane (Piramal Healthcare, Andhra Pradesh, India) and placed into a stereotaxic apparatus in flat-skull position and injected bilaterally using a 30 gauge cannula (8.0mm, Plastics One, Roanoke, VA) targeted to the SON according to a stereotaxic atlas[68]. An

adeno-associated virus (AAV) construct containing mouse AVP gene promoter and EGFP reporter, received from the laboratory of Harold Gainer (NIH, Bethesda, MD) and constructed by UNC Gene Therapy Center (Chapel Hill, NC) was used to visualize AVP MNCs within the SON of each rat. Stereotaxic microinjections of 0.6 ul of recombinant AAV construct will be bilaterally injected into each SON at a rate of 0.25ul/min. Following the injection, rats will be allowed two weeks for recovery time and adequate vector expression.

2.4 Immunohistochemistry

Rats were deeply anesthetized with inactin (100mg/kg, i.p.), perfused transcardially with phosphate-buffered saline (PBS) followed by 4% paraformaldehyde in PBS. After the perfusion, brains were extracted from the skull and placed in 30% sucrose until dehydrated. To prepare brains for immunohistochemistry, the forebrain and hindbrain were serial sectioned at 40um-thickness and separated into three groups. Sections were processed for AVP guinea pig polyclonal Anti-(Arg^8)-VP (1:1,000; Cat# T-5048 Peninsula Labs, San Carlos, CA, USA), anti-KCC2 rabbit monoclonal IgG (information provided above) and OXT anti-oxytocin mouse monoclonal IgG (1:10,000; Cat# MAB5296, Millipore, Billerica, MA, USA). Sections were incubated in primary antibodies for two days at 4^oC. Following primary antibody incubation, sections were then rinsed with PBS salt solution, followed by sequential incubation in respective secondary antibodies against host species conjugated to CY3 fluorophores (CY3-conjugated anti-guinea pig IgG (1:10,000; Cat# 706-165-148, Jackson); Cy3-conj. Affinipure Anti-Mouse IgG (1:10,000; Cat#715-165-151, Jackson); CY2-conj. AB Anti-rabbit IgG (1:10,000; Cat# 711-225-152, Jackson)). Sections were then rinsed again in PBS solution and mounted on gelatin coated

slides, then cover slipped with hard set Vectashield (Vecta Labs, Burlingame, CA, USA) mounting media.

Sections containing the SON were analyzed for vasopressin and KCC2 expression to confirm chloride extruder expression in MNCs displaying vasopressin immunofluorescence. Sections containing AAV-AVP vector expression by EGFP reporter were analyzed for AVP or OXT immunofluorescence to confirm vector transfection success and specificity.

2.5 In Vitro Electrophysiological Recordings

Coronal hypothalamic slices containing the SON were prepared from EU control and 48-hour WD rats. Each rat were anesthetized with isofluorane and decapitated. The brain is rapidly removed and placed in ice cold, oxygenated (95% O_2, 5% CO_2) cutting solution (in mM) KCl 2, $MgCl_2$-$6H_2O$ 1, $CaCl_2$ 2, $MgSO_4$ 2, NaH_2PO_4 1.25, $NaHCO_3$ 26, D-Glucose 10, Sucrose 206. Coronal sections 300 um thick were cut with a Microslicer DTK Zero 1 (Ted Pella, Inc.) and double-sided silver blue razor blade (Gillette). Slices were incubated at room temperature for forty-five minutes prior to recording in oxygenated (95% O_2, 5% CO_2) ACSF composed of (in mM) NaCl 126, KCl 3, $CaCl_2$ 2, $MgSO_4$ 2, NaH_2PO_4 1.25, $NaHCO_3$ 26, and D-Glucose 10 (300mOSM/kg H_2O) adjusted to a pH of 7.4 with NaOH. Cells were visualized on a black and white monitor (Panasonic) and EGFP fluorescence was visualized using cellSens Dimension 1.6 software (Olymus). Whole-cell patch clamp techniques and recordings were performed on an upright epifluorescent microscope (BX50WI, Olympus) equipped with perfusion system containing perfusion solution: ACSF + tetrodotoxin (0.5 uM; Cat# 1078, Tocris, Ellisville, MO) + bicuculine methbromide (10 uM; Cat# B7561; Sigma) to isolate mEPSCs. mEPSCs were recorded using Axopatch-1A and Digidata 1440A (Axon Instruments), and signals were sampled

at 2 KHz and digitized at 10KHz. pipettes were pulled from borosilicate glass (3-6MΩ) and contained internal solution composed of (in mM) CsCl 130, NaCl 10, HEPES 10, EGTA 1, Na_2ATP 2, NaGTP 0.4. Recordings from identified AVP MNCs were made by targeting eGFP-expressing neurons in slices prepared from rats injected with the AAV-AVP virus.

Following whole-cell access, cells were clamped in a slightly depolarized state of -55mV in order to remove Mg^{2+}-dependent inactivation and measure NMDA receptor (NMDAR) contribution to mEPSCs[19,33,41]. Stable baseline was recorded for 3 – 5 minutes from spontaneous mEPSCs, then NMDAR and AMPAR-mediated components were pharmacologically isolated with drug application for 5 minutes. Application of AMPA antagonist CNQX (10uM; Cat# 0190; Tocris) allowed for isolation of NMDAR contribution. Parameters measured for mEPSCs were amplitude, rise time (ms), decay time (ms), charge transfer, and with drug application, mEPSC frequency was also measured at baseline and with CNQX application, with equal time segments taken for each frequency measurement (Fig 1).

2.6 SON Dissociation

Rats were anesthetized with isofluorane and decapitated. Brain was isolated and placed ventral side facing up in ice cold ACSF (recipe noted above) underneath a dissecting microscope. Using forceps and microscissors, the SON was isolated and harvested from either side of the optic chiasm and placed in a drop of Hibernate A (Cat# A12475-01, Gibco, Grand Island, NY, USA). Once both SON were harvested and in Hibernate A drop, tissue was transferred to a tube containing CaCl2-free Hibernate medium (Cat# HA-Ca, BrainBits, Springfield, IL, USA) and proteolytic enzyme papain (Cat# 3119, Worthington, Lakewood, NJ, USA), which was then allowed to incubate in water bath at 31^{o}C for thirty minutes. Following

incubation, cells were allowed to settle, supernatant was discarded and then began the process of mechanical dissociation. The cell pellet was washed in Hibernate A medium and was triturated for three washes to mechanically dissociate. The tube was then centrifuged (Centrifuge 5418R, Eppendorf) at room temperature at 1100rpm for 8 minutes and the cell pellet isolated. Neurobasal A (Cat# 10888-022, Gibco)/B27 (Cat# 17504, Invitrogen) stock solution, also containing GlutaMAX media standard (20 uM; Cat# 35050-061, Invitrogen) and penicillin-streptomycin antibiotic cocktail, Penstrep (Cat# 15140-22, Gibco) was added to pellet which was gently triturated. Final Neurobasal A/B27-cell mixture was then plated into four 35mm glass-bottomed plates coated with PolyD Lysine (100ug/ml; Cat# P6407, Sigma) to promote cell adhesion to plate. Plates were then incubated for 24 hours.

2.7 Ratiometric Calcium Imaging

On the day of the experiment, cells are washed in HBSS (Cat# 14025-092, Gibco) composed of (in mM) 1.26 $CaCl_2$, 0.49 $MgCl_2 \cdot 6H_2O$, 0.4 $MgSO_4 \cdot 7H_2O$, 5.3 KCl, 0.44 KH_2PO_4, 127.9 NaCl, 0.33 $Na_2HPO_4 \cdot 7H_2O$, 5.5 D-Glucose and pH of 7.4. One hour prior to start of experiment, cells were incubated in a calcium-sensitive dye Fura 2AM (2 uM; Cat# F1221, Invitrogen, Eugene, OR, USA) and pluronic acid (1.5 mM; Cat# 84-094-00, Cellomics, Thermo Fischer Scientific) in Neurobasal A/B27 cocktail described earlier. Cells were then washed in HBSS twice. The coverslip was then mounted onto the stage of an inverted microscope (Olympus IX81, Olympus, Melville, NY)and cells were excited at wavelengths alternating between 340 nm and 380 nm using a xenon light source (Lumen200Pro, Prior Scientific, Rockland, MD, USA) to obtain ratiometric data. The emitted light was captured at 520 nm wavelength with a CCD camera (Hamamatsu camera controller C10600, Hamamatsu Photonics

KK, Hamamatsu, Japan) and pixel data was binned (2X2) and images captured every two seconds. Ratiometric data was captured and analyzed using Slidebook software (Slidebook 5.0, Intelligent Imaging Innovations, Denver, CO, USA). After achieving two minutes of stabilized baseline, cells were stimulated with 10 uM AMPA and then 20uM AMPA with sufficient time allowed between drug applications for response to recover or plateau. Ratio values were then normalized to the baseline values averaged over one minute before drug application proceeded. For each cell recording, the normalized change from baseline was determined, and data from an entire coverslip was averaged for every individual experiment, and treated as one data point. At the end of each experiment, the coverslip was exposed to ionophore ionomycin (5 uM; Cat# 10634, Sigma) to determine a maximum response and to determine inclusion criteria for cells on each coverslip. Cells that did not take up calcium-sensitive Fura 2AM dye or did not respond to ionomycin were excluded from analysis. In coverslips that contained MNCs displaying GFP+ and GFP- labeling, the GFP+ MNCs and GFP- MNCs were analyzed separately. In order to remain conservative in our inclusion criteria of GFP+ fluorescing MNCs on coverslips, the cell had to display fluorescence when viewed under the microscope's FITC fluorescent filter specifically. If there was no fluorescence observed under the FITC filter, or if the signal leaked over to TXRED fluorescent filter, the MNC was excluded from GFP+ MNC analysis group. In coverslips that did not contain GFP-labeled MNCs, these data were analyzed separately from individual GFP+ and GFP- responses.

2.8 Statistics

For immunohistochemistry, the number of cells double-labeled with EGFP were manually counted, and double labelling of AVP-GFP and OXT-GFP were calculated and

expressed as a percentage. Electrophysiological recordings were manually analyzed using Clampfit and MiniAnalysis software. Comparisons between treatment groups were performed using a one way ANOVA with Holm-Sidak post hoc tests for multiple comparisons. Two way ANOVAs with Holm-Sidak post hoc determined significance between GFP+ and unlabeled MNCs, and for patch-clamp experiments with drug application of CNQX, two way repeated measures ANOVA tests with Student Newman Keuls post hocs were carried out for stepwise multiple comparisons. Statistical analysis was performed with SigmaPlot 12.0 software. Ratiometric calcium imaging experiments were analyzed and reported as treatment means $\pm$ SE. Data was analyzed by three-way ANOVA with Holm-Sidak post hoc tests performed as necessary. Significance was reported as a value of $P < 0.05$.

RESULTS

3.1 Identification of vasopressin and oxytocin neurons

In order to distuinguish OXT from AVP magnocellular neurons, we injected an AAV2 vector (p2.OVIP.EGFP) with an AVP promoter and eGFP reporter targeted to the SON. Previous studies have shown the specific expression of eGFP in AVP neurons in the SON[69]. To confirm these previous findings, brains of injected rats were prepared for immunofluorescence in separate sections of coronal slices containing the SON. Sections were processed for either AVP or OXT immunohistochemistry using a Cy3-conjugated secondary antibody. Colocalization of GFP with either AVP or OXT was determined by light microscopy and percent double-labeling was calculated. Our results indicate the colocalization of GFP and AVP MNCs in the SON (89% GFP-AVP double labeling, n=3) (Fig. 2) and not GFP and OXT (0.08% GFP-OXT double labeling, n=3) (Fig. 3) ($p \leq 0.001$). Given this demonstration of successful vector transduction, we can conclude that the AAV2 vector is selective to AVP expressing MNCs, enabling us to distinguish AVP versus OXT MNCs in the SON. This capability permitted further differentiation of neuronal types and their respective electrophysiological properties during patch-clamp studies (Fig. 4).

3.2 Water deprivation effect on mEPSPs of AVP MNCs in SON

Patch-clamp electrophysiological recordings were obtained from a total of 58 SON MNCs obtained from EU (GFP+ MNCs n = 6; unlabeled MNCs n=13), 24H WD (GFP+ MNCs

n = 5; unlabeled MNCs n=13), and 48H WD rats (GFP+ MNCs n = 6; unlabeled MNCs n=15). To study WD-mediated changes in mEPSCs, patch-clamp recordings (voltage-clamp mode) were obtained from coronal brain slices containing the SON that had been injected with AAV2-AVP vector (Fig. 4). As shown in Fig. 5 and Table 1A, GFP+ MNCs in slices exposed to 48H WD treatment exhibit significantly greater mEPSC amplitude than those exposed to EU or 24H WD treatment ($p < 0.05$). While other measured parameters in GFP+ MNCs were trending to increase with 48H WD challenge, the measured rise, decay, and charge transfer were not found to be statistically different from those of EU and 24H WD treatment groups, potentially due to the small sample sizes.

Among the unlabeled MNC population of recordings, we did not observe significant increases with 48H WD (Table 1B). Worth noting are the significant differences in the rise time ($p < 0.05$), decay time ($p < 0.001$), and charge transfer ($p < 0.001$) of GFP+ MNCs compared to unlabeled MNCs when exposed to 48H WD treatment.

3.3 Water deprivation enhances AMPAR contribution to mEPSPs of MNCs in SON

To study the changes in excitatory neurotransmission we observed in SON MNCs with increasing WD homeostatic challenge, patch-clamp electrophysiological recordings with AMPAR antagonist CNQX administration were obtained from a total of 12 unlabeled SON MNCS from EU (n = 7) and 48H WD rats (n = 5). Fig. 6 shows trace excerpts of an unlabeled EU MNC at baseline (Fig. 6A) and with CNQX application (Fig. 6B), and Fig. 7 shows trace excerpts from a 48H WD unlabeled MNC at baseline (Fig. 7A) and with CNQX application (Fig. 7B). We observed a significant decrease in the frequency of mEPSCS with CNQX application in both treatment groups ($0 < 0.05$) while analyzing equal time segments within recordings, and the

decrease in frequency of mEPSCs appeared to be more pronounced in the 48H WD group (Fig. 8). While conducting these experiments, we were unable to successfully record from MNCs that displayed GFP fluorescence. As a result, we were unable to replicate the increase in mEPSC parameters observed in Table 1A, and the data from these experiments more closely resembles data shown in Table 1B. Therefore, there were no differences in the baseline measured mEPSC parameters between treatment groups, hence we did not see any significant changes with CNQX application between treatment groups (Table 2). in order to better evaluate and understand changes observed in previous experiments, we would need to increase sample sizes of both treatment groups, and record from GFP+ labeled MNCs.

3.5 Ratiometric Calcium Imaging of EU and 48H WD SON MNCS

To supplement electrophysiological recordings, ratiometric calcium imaging was performed on dissociated SON MNCs that had been exposed to either EU (total coverslips analyzed n=19; GFP+/GFP- coverslips n=12) or 48H WD (total coverslips analyzed n= 12; GFP+/GFP- coverslips n=6) treatment in animals that had been injected with AAV2-AVP virus. Presence of GFP-labeled MNCs confirmed a successful injection, and coverslips that contained GFP+ and GFP- MNCs (Fig. 9) were analyzed separately (Fig. 12) from coverslips that contained unlabeled MNCs. Cells included in analysis of each coverslip demonstrated successful uptake of the calcium-sensitive Fura 2AM (Fig. 10A) and responsiveness to ionophore ionomycin (Fig. 10B). An example of traces collected from a single coverslip with applications of 10uM AMPA, 20uM AMPA, and ionomycin with respective changes in calcium influx shown by changes in 340nm/380nm ratio are shown in Fig. 11. The normalized Δ in cytosolic calcium concentration from baseline in GFP+ and GFP- MNCs exposed to EU or 48H WD treatment

with applications of 10uM and 20uM AMPA are shown in Fig. 12. We observed a significant increase in cytosolic calcium mobilization in GFP+ as compared to GFP- MNCs ($p < 0.001$), a surprising and significant decrease in calcium mobilization with 48H WD treatment ($p < 0.05$), and a significant increase in intracellular calcium mobilization with increasing concentrations of applied AMPA ($p < 0.05$), but these changes were independent of all other variables (Fig. 12). There were no significant interactions between cell type and hydrational status. Some coverslips showed no GFP fluorescence in any MNCs and being putative viral vector injection misses, these coverslips were analyzed separately. Therefore we also analyzed data independent of GFP fluorescing MNCs in order to include responses measured in coverslips whose cells could not be identified as putative vasopressin or oxytocin-expressing MNCs. When the total response of all calcium experiments in both EU and 48H WD treatments was compiled, we observed a similar responses as observed in Fig. 12 where MNCs exposed to 48H WD exhibited significantly smaller responses to AMPA as compared to EU MNCs (WD 0.21 ± 0.06, EU 0.38 ± 0.04). Once we included coverslips that had not had any GFP fluorescing MNCs, we observed statistically significant differences between the 10uM and 20uM AMPA doses ($p < 0.05$) but not between treatment groups (10 uM 0.23 ± 0.05, 20 uM 0.37 ± 0.05). This suggests that in order to better evaluate changes in SON MNC calcium influx with 48H WD treatment, we would need to increase our sample size and modify our experimental setup to include fast Na+ channel blocker, tetrodotoxin as well as calcium channel antagonists in the incubation solution to selectively isolate and measure calcium influx through AMPAR and/or NMDARs only.

DISCUSSION

The regulation of the release of AVP from the posterior pituitary is critical in its contribution to the maintenance of body fluid homeostasis, however the mechanisms by which this happens is not clearly understood to date. With the use of this WD model presenting a homeostatic challenge to blood volume and plasma osmolality, we were able to determine that 48H WD does indeed effect excitatory neurotransmission of AVP MNCs in the SON in a way that is measurably distinct from the response of the SON MNC population as a whole. Our results show increases in GFP+ and a trend towards increase in unlabeled MNC mEPSC amplitude with 48H WD treatment, however the increase in amplitude with WD treatment is statistically significant in only the GFP+ MNCs. More data will need to be collected in the unlabeled MNC population to determine if trends are authentic. We also observed increases in mEPSC parameters of rise time, decay time, and charge transfer with 48H WD in GFP+ MNCs that were significantly different from the changes seen in the same treatment group of unlabeled MNCs. This data suggest that pathways mediated by this homeostatic challenge alter excitatory neurotransmission of AVP MNCs in the SON. However, these trends towards increased rise time, decay time, and charge transfer were not duplicated successfully in experiments involving AMPAR antagonist CNQX.. More data in GFP+ labeled and unlabeled SON MNCs is still needed to sufficiently determine how these changes are mediated by NMDAR contribution to glutamatergic activity. Data from experiments using CNQX application appear to be more similar to data in patch-clamp experiments where mEPSCs from unlabeled MNCs were

recorded. Here we did not see the same increases in mEPSC amplitude and charge transfer as observed in GFP+ MNCs exposed to 48H WD treatment.

Interestingly, the data collected from ratiometric calcium imaging suggests with 48H WD, there is less influx of calcium across the plasma membrane of AVP MNCs, which challenged the expectations we had after observing the enhanced of mEPSC parameters with 48H WD in the patch-clamp studies. While the GFP+ MNCs did exhibit higher levels of cytosolic calcium mobilization as compared to GFP- MNCs, this effect was independent of the other treatments. One potential explanation for this is in experimental preparation that comes with dissociating neurons. By dissociating SON MNCs, you remove presynaptic, dendritic, and astrocytic connections and influence in proximity to MNCs. These connections tend to be better preserved in tissue slice and explant preparations. The influence of neighboring astrocytes, specifically, have been shown to effect excitatory modalities in the SON by astrocytic extrasynaptic NMDARs that evoke a tonic, persistent form of excitation to MNCs and thereby mediate excitatory neurotransmission[18]. Dehydration has been shown to cause the retraction of astrocytic processes which functionally removes glutamate transporters from the synapse and thereby influences glutamate neurotransmission in MNCs. Increased extracellular glutamate has been proposed to trigger changes in synaptic strength associated with dehydration. By dissociating MNCs for the calcium imaging experiments, we may have eliminated a potential source required for changes in glutamate neurotransmission regulation[18]. Enzymatic dissociation of MNCs could potentially sever MNC dendritic networks from which neurotransmitter is released. Dendritic release of AVP, OXT, and other neuropeptides has been shown to influence rhythmic activity patterning in MNCs, and even more recently, it has been shown to coordinate activity through an NMDA-mediated increase in dendritic calcium signaling[14,70]. By dissociating

SON MNCs, our results may reflect the isolation of MNCs from these astrocytic, dendritic, and presynaptic influences known to normally influence their activity. A last potential explanation for these surprising results observed with ratiometric calcium imaging comes again in the experimental preparations. Between the dissociation and the actual calcium experiment, the dissociated MNCs were incubated for twenty-four hours because cells appear healthier in our preparations that have been allowed this particular incubation protocol. However, this incubation period may have allowed for adequate recovery from the physiological challenge and the decrease in cytosolic calcium mobilization we observed after 48H WD may be attributed to this. In order to determine if this is the case, we may need to determine if cell vitality has not been compromised at earlier incubation times, so as to guarantee the responses we are observing in calcium experiments are results of the homeostatic water deprivation challenge.

Additional data is still needed to determine if observed trends are indeed attributed to WD-mediated changes in excitatory neurotransmission. It would also be advisable to add TTX to our dissociated MNC bath solution in order to inhibit fast sodium channels and calcium channel blockers, which, if an action potential is generated, would be responsible for opening voltage-sensitive calcium channels, which would confound data.

With continued study of WD mediating excitatory neurotransmission in AVP MNCs through patch-clamp electrophysiology and ratiometric calcium imaging to measure mEPSCs and calcium mobilization, we would continue to expand our understanding of alterations in excitatory neurotransmission in this model. In order to determine if the trends we observed for WD increasing mEPSC parameters in OXT and AVP MNCs are indeed significant, we will need to collect mEPSC recordings from GFP+ labeled MNCs and additional unlabeled MNCs with CNQX application.

Overall, the modifications in mEPSCs observed with the WD homeostatic challenge are consistent with what was predicted and will help the scientific community gain a better understanding of how these changes could be affected by intracellular signaling pathways postsynpatically in the SON. Equally as important as understanding the alterations in excitatory neurotransmission that take place under this physiological stressor is determining the pathways involved in regulating these changes. Isolating NMDAR components of glutamatergic neurotransmission in SON MNCs would provide additional insight, as would targeting pathways proposed responsible for these observed changes, since mechanisms of regulation are poorly understood.

Along with isolating changes in excitatory neurotransmission of AVP MNCs with exposure to WD, the inhibitory portion of control of release of AVP must also be addressed. Leng's model of the effect of plasma osmolality on AVP release states there is a linear relationship between plasma osmolality and plasma AVP[10]. This proposes that the balance of synaptic excitatory and inhibitory inputs determine the linear relationship, so increases in excitatory drive could also be balanced a simultaneous increase in inhibitory drive. Monitoring changes in GABAergic neurotransmission with WD challenge would be particularly interesting in AVP MNCs, and future direction would involve perforated-patch clamp methods to measure mIPSCs. Surrounding GABAergic neurotransmission in MNCs, there is a particular amount of controversial findings within the scientific society currently[18,24,33,35]. There are several theories surrounding the control of AVP release and network influences on glutamatergic and GABAergic signaling. Gaining a functional understanding of the changes in neurotransmission and pathways responsible will allow us to move forward to challenge pathophysiological models known to lead to the inappropriate release of AVP seen with disease states such as liver cirrhosis

and congestive heart failure. Elucidating mechanisms of sustained AVP release, and analyzing molecular pathways that influence excitatory and inhibitory inputs is important in unveiling mechanisms of neural plasticity and also with disease-associated functional changes that may be occurring.

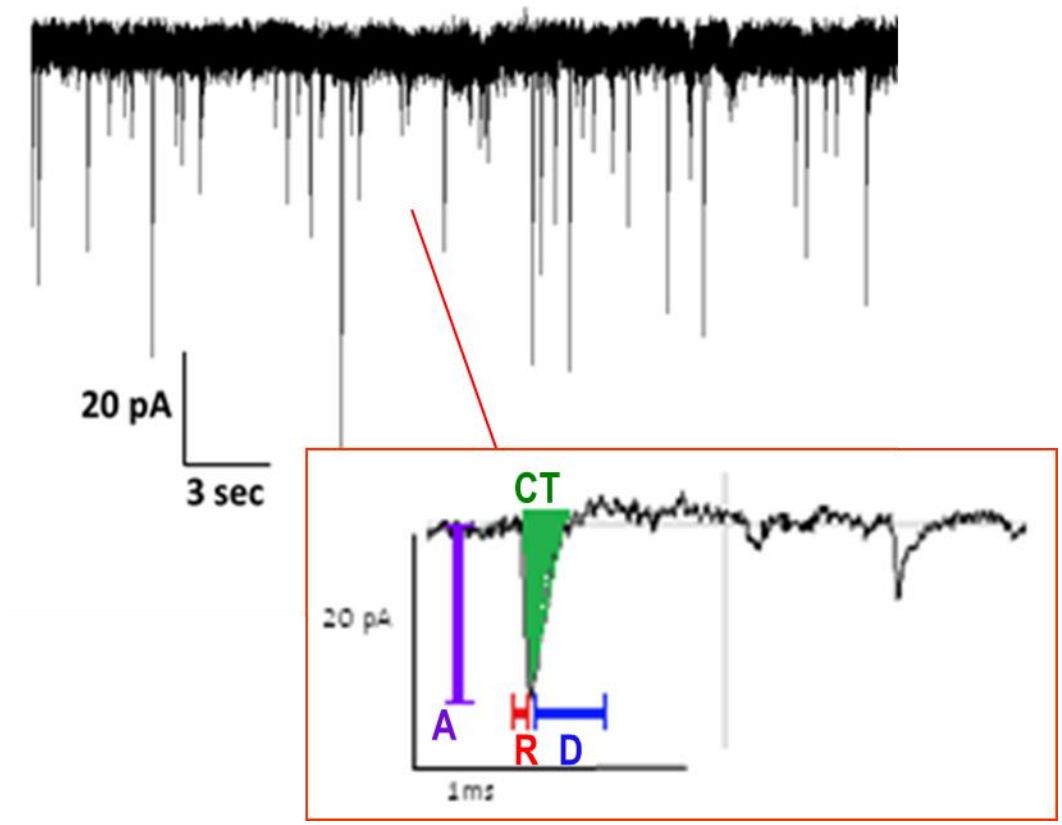

Figure 1. Example recording and segment showing mEPSC parameters measured. A indicates amplitude (pA) and is a measures current change from baseline to peak mEPSC and could indicate changes in AMPAR trafficking to the membrane. R indicates rise time (ms) and measures time taken to peak mEPSC, D indicates decay time and measures time from mEPSC peak to baseline. Both these measurements could indicate changes in subunit expression of NMDARs. CT indicates charge transfer and is associated with the area under the mEPSC depolarization, which could be indicative of either NMDAR or AMPAR influence.

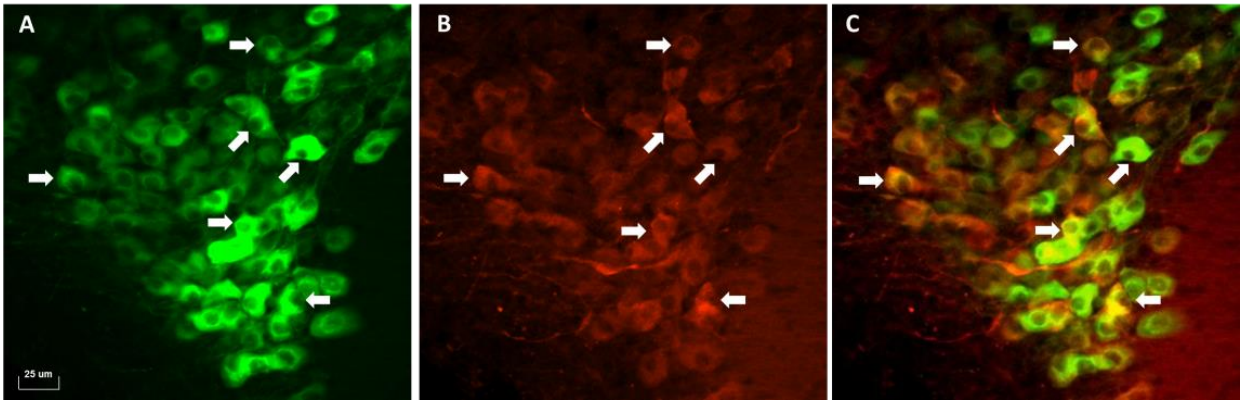

Figure 2. Immunofluorescence of AAV-AVP-GFP virus (A) and CY3-labeled AVP neurons (B) within the SON. A merged digital image indicates overlap of fluorescence colored yellow (C). Cells labeled with GFP and AVP are indicated with arrows. Scale bar = 25 um.

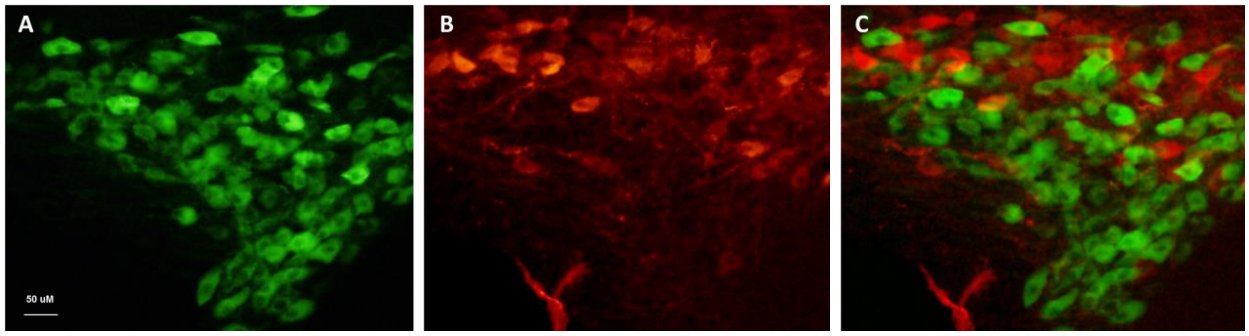

Figure 3. AAV-AVP-GFP Virus Expression and CY3-labeled OXT Neurons. Immunofluorescence of AAV-AVP-GFP virus (A) and CY3-labeled OXT neurons in red (B) within the SON. A merged digital image (C) shows GFP and CY3-labeled cells are mutually exclusive. Scale bar = 50 um.

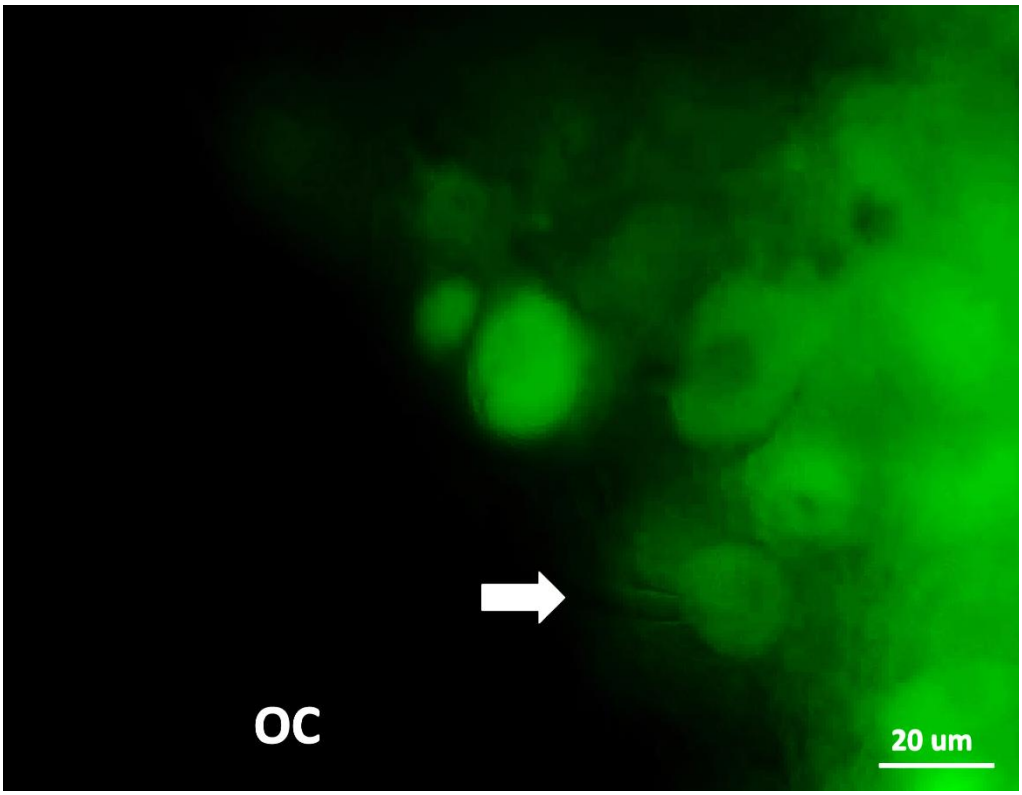

Figure 4. Immunofluorescence of patched GFP+ labeled cell during patch clamp experiment. Magnification at 40X, scale bar = 20um. 'OC' denotes optic chiasm and arrow indicates the tip of glass patch pipette.

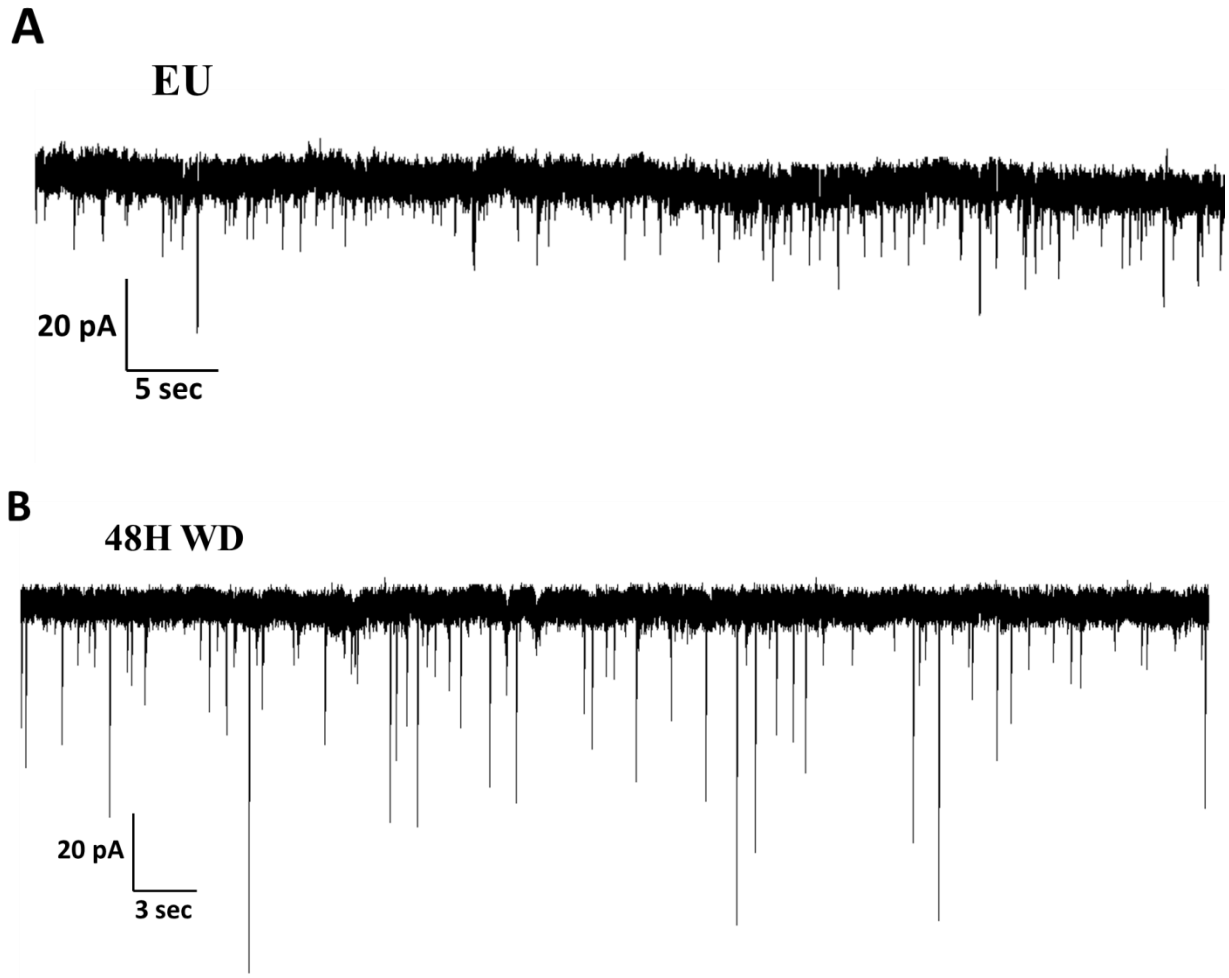

Figure 5. Example trace obtained from patch clamp recording of an unlabeled SON MNC from EU rat (**A**) and a GFP+ SON MNC from 48H WD rat (**B**).

Table 1. Electrophysiological parameters measured in GFP+ and unlabeled SON MNCs exposed to EU, 24H or 48H WD treatment groups.

A GFP+ MNCs	EU	24H WD	48H WD
n	6	5	6
Amplitude	11.221 ± 0.461	11.020 ± 0.062	13.238 ± 0.896*
Rise (ms)	1.998 ± 0.147	1.922 ± 0.110	2.137 ± 0.228 *
Decay (ms)	3.371 ± 0.262	3.901 ± 0.110	4.551 ± 1.010 **
Charge Transfer	40.577 ± 4.572	44.853 ± 4.389	57.551 ± 10.623 **

B Unlabeled MNCs	EU	24H WD	48H WD
n	13	13	15
Amplitude	11.921 ± 0.483	12.416 ± 0.651	13.424 ± 0.683
Rise (ms)	1.742 ± 0.082	1.900 ± 0.114	1.697 ± 0.056
Decay (ms)	3.085 ± 0.322	3.223 ± 0.423	2.406 ± 0.149
Charge Transfer	38.321 ± 3.074	40.226 ± 3.785	34.542 ± 1.312

Recordings were obtained from MNCS from EU, 24H, and 48H WD rats. Patched cells were characterized as GFP-labeled (GFP+) (**A**) or unlabeled (**B**). Measured parameters within cell type were compared using a one way ANOVA with Holm-Sidak post hoc for multiple comparisons. Measurements between GFP+ and unlabeled MNCs were compared using a two way ANOVA with Holm-Sidak post hoc for multiple comparisons. Data reported as mean ± SEM. * indicates $p < 0.05$, ** indicates $p < 0.001$ from unlabeled MNCs

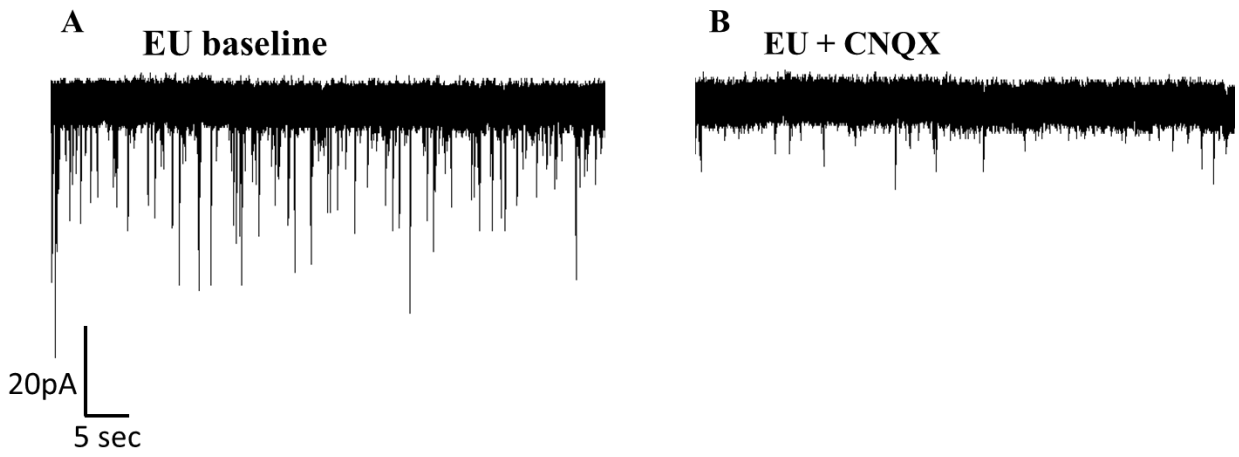

Figure 6. Trace excerpt of recording of EU unlabeled SON MNC at baseline (**A**) and CNQX application (**B**).

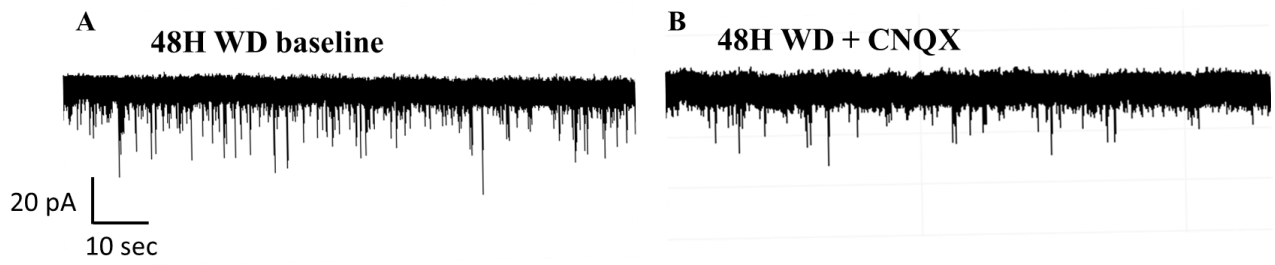

Figure 7. Trace excerpt of recording of 48H WD unlabeled SON MNC at baseline (**A**) and CNQX application (**B**).

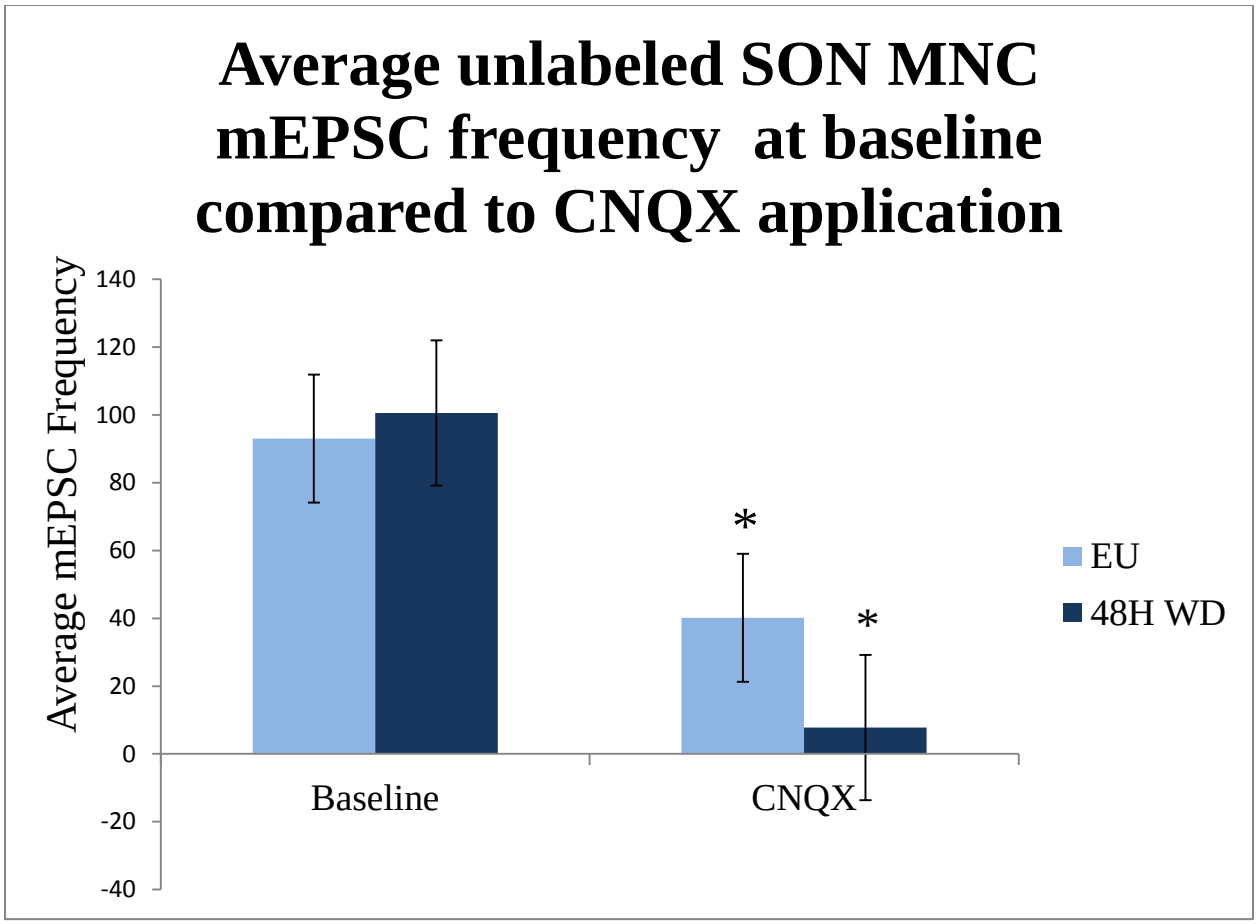

Figure 8. Frequency of mEPSCs in unlabeled SON MNCs decrease with application of CNQX in EU and 48H WD treatment groups. Data shows the averaged frequency of mEPSCs observed in one minute of trace recording during baseline and CNQX drug application. * $P < 0.05$ respective to treatment baseline measurements.

Table 2. Response of unlabeled SON MNCs to application of AMPAR antagonist CNQX after exposure to EU or 48H WD treatment.

	EU		48H WD	
	Baseline	CNQX	Baseline	CNQX
n	7		5	
Amplitude	12.555 ± 0.873	11.651 ± 0.873	12.653 ±1.033	10.335 ± 1.033
Rise (ms)	1.744 ± 0.097	2.263 ± 0.097	1.730 ± 0.114	2.471 ± 0.114
Decay (ms)	3.027 ± 0.408	4.515 ± 0.408	2.666 ± 0.483	4.587 ± 0.483
Charge Transfer	39.625 ± 5.546	52.405 ± 5.546	33.948 ± 6.562	50.228 ± 6.562

Recordings were obtained from unlabeled SON MNCs exposed to EU or 48H WD treatment. Parameters were measured at baseline and with CNQX drug application. Data comparisons within recordings and between groups were analyzed by two way repeated measures ANOVA with Student-Newman-Keuls post hoc analysis, and presented as mean ± SEM.

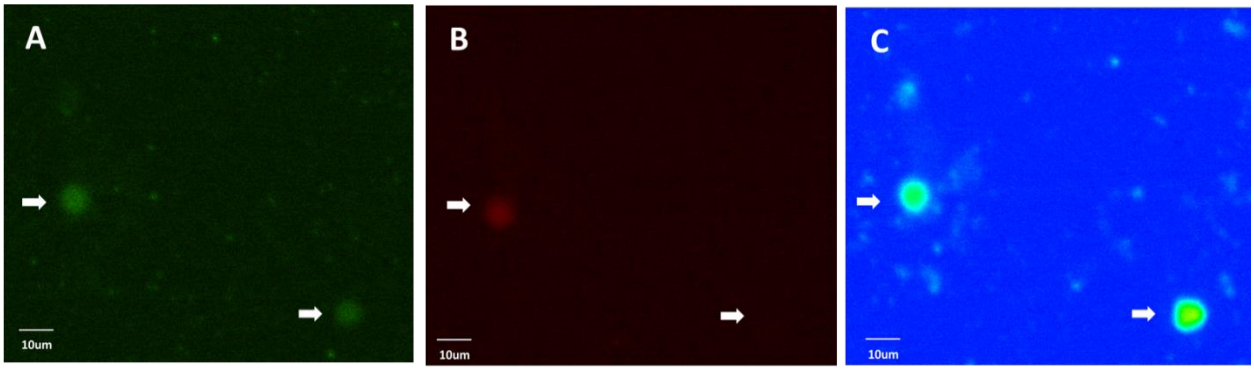

Figure 9. Two dissociated SON MNCs loaded with Fura 2AM indicated by arrows. **A** Shows MNCs under FITC filter, **B** shows MNCs under TXRED filter to determine specificity of GFP labelling. From the TXRED filter it is confirmed that one of the pictured MNCs is positively labeled with GFP flourophore because of its specifity to FITC filter and not TXRED filter (bottom right cell). **C** shows MNCs in 340 filter confirming the MNCs are loaded with Fura 2AM dye.

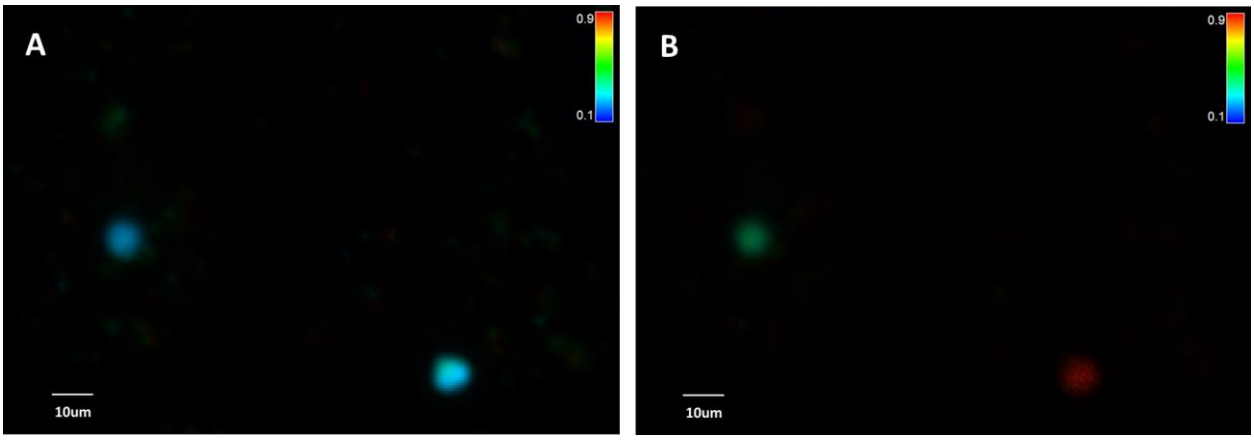

Figure 10. Representative of two cells shown in Figure 8 pseudocolored to show 340nm to 380nm ratio changes at baseline (**A**) and at maximum calcium response to ionomycin (**B**). The inset table color scale depicts changes in the 340nm to 380nm ratio (0.1 – 0.9). Scale bar = 10um.

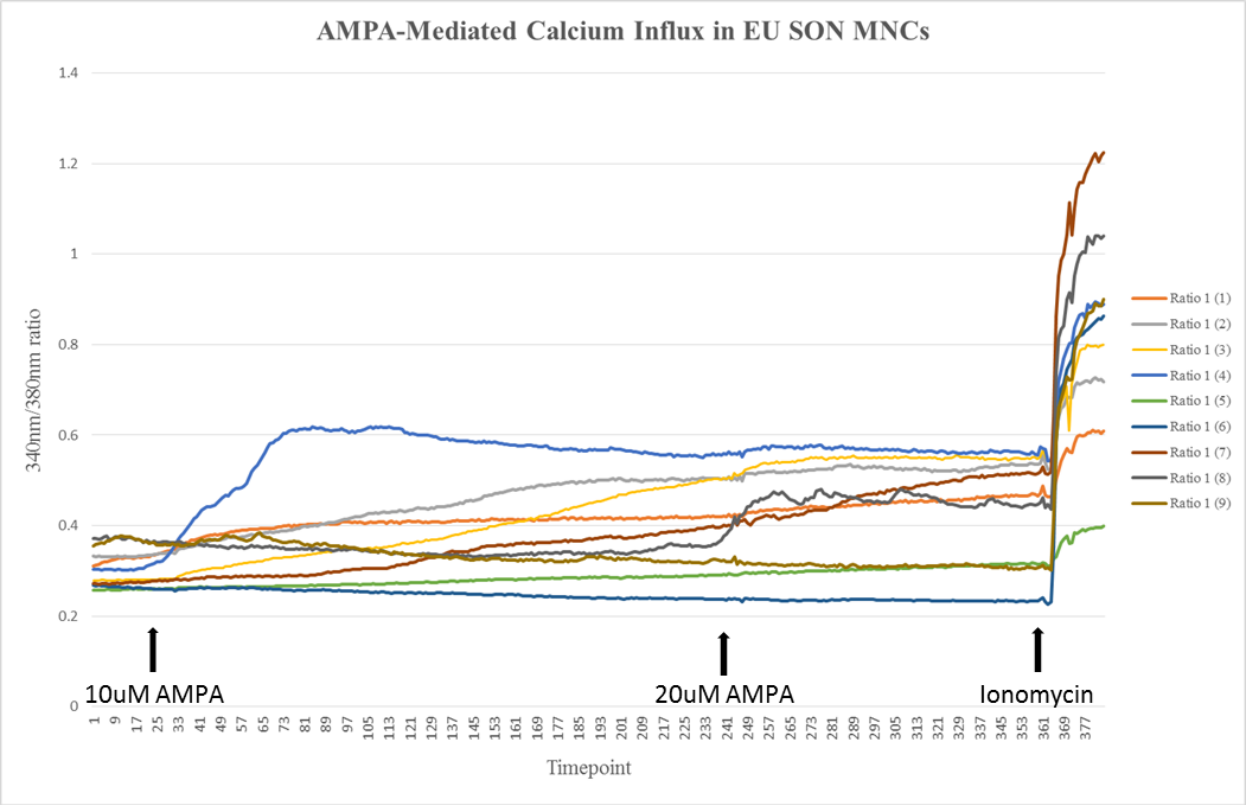

Figure 11. Example traces of AMPA-induced increases in intracellular calcium in dissociated SON MNCs. Ratios 2, 3, and 4 depict GFP+ dissociated MNCs. Drug application indicated by arrows.

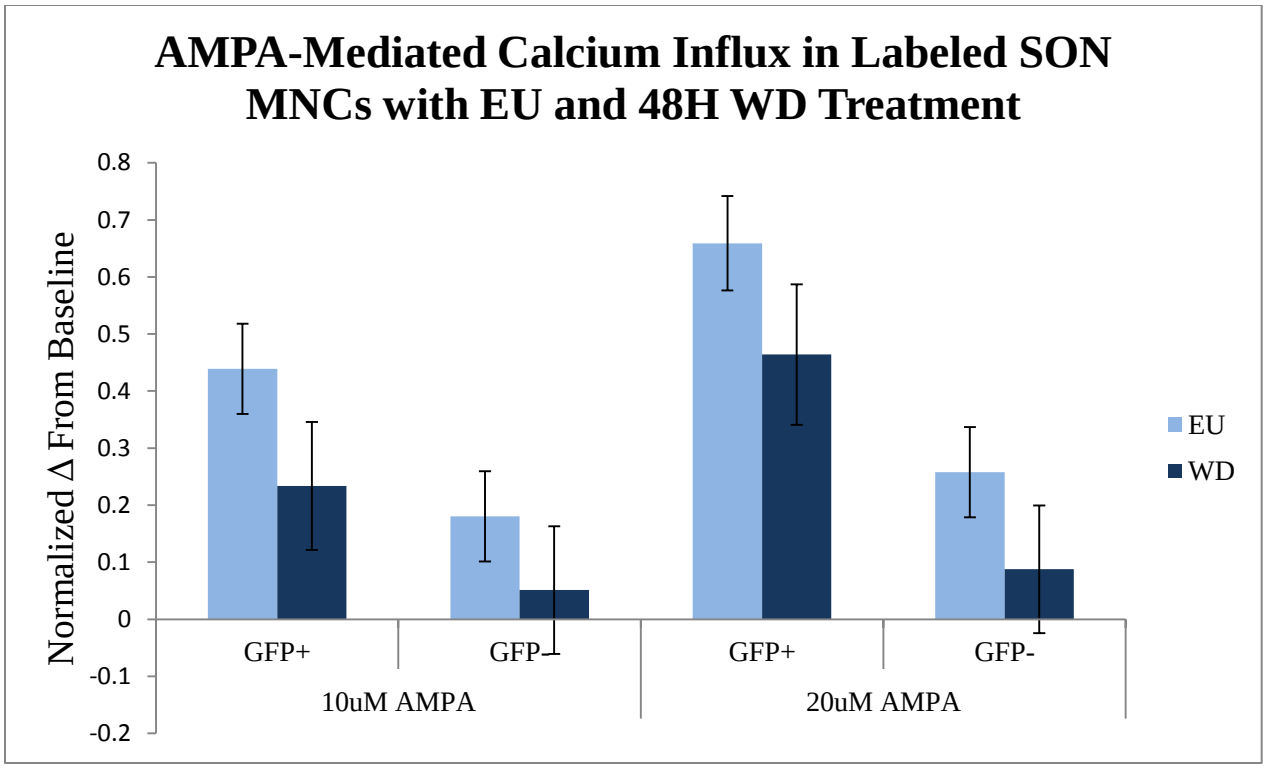

Figure 12. AMPA-increased intracellular calcium in dissociated SON MNCs normalized to baseline in GFP+ and GFP- MNCs exposed to either EU treatment (n=12) or 48H WD (n=6). The difference between the mean baseline ratio and maximal ratio (**Δ** 340nm/380nm) was measured using a three way ANOVA and Holm-Sidak pairwise multiple comparisons tests. There were statistically significant increases in the responses of GFP+ versus GFP- labeled MNCs ($p < 0.001$), increased calcium mobilization in EU as compared to 48H WD treatment groups ($p < 0.05$), and increased responses to the applied doses of AMPA (10mM vs. 20 uM) as a whole ($p < 0.05$) but there were no significant interactions among treatments.

Appendix

Materials and Methods

Micropunch Dissection and SON Tissue Lysate Preparation

Rats were anesthetized with inactin (100mg/kg i.p.) and decapitated. The brain was then rapidly removed from the skull and placed in a commercially available brain matrix (Stoelting Wood Dale, IL, USA) kept cold using ice. The matrix was used to section the brain into 1 mm coronal slices with the use of double-edged razor blades. Slices containing the SON were then placed on a bed of dry ice and punches of the SON were collected using 1 ml syringes equipped with blunt 23-guage needles. Punched samples were then placed in microcentrifuge tubes, rapidly frozen, and stored at -80^{o}C until further processing.

Punches were sonicated in 35ul of modified cell lysis reagent RIPA-buffer, supplemented with protease and phosphatase inhibitors followed by a 30 minute incubation on ice. The total homogenates were centrifuged at 12000 RPM for 20 minutes at 4^{o}C to clear the lysate, and the supernatant (total lysate) was transferred to new clear microcentrifuge tubes.

Western Blot

Total protein concentration of lysate was determined using the Bradford method [71]. 20 – 40 ug of total lysate were loaded onto a 7.5% sodium dodecyl sulfate (SDS)-polyacrylamide gel, electrophoresed in Tris-glycine buffer under denaturing conditions and then transferred to

nitroceullulose membrane (BioRad, Hercules, CA, USA) in Tris-glycine buffer with 10-20% methanol. Membranes were blocked for 1 hour at room temperature with 5% (wt./vol.) nonfat milk in Tris-buffered saline 0.05% (vol./vol.) Tween 20 (TBST-Tween; 50 mM Tris base, 200 mM NaCl, 0.05% Tween 20.) Membranes were then incubated overnight at 4^{o}C with primary antibody in blocking solution (recipe noted above). Primary antibodies were: KCC2 rabbit polyclonal ab. (Cat# 07-431 Millipore, Billerca, MA, USA), NKCC1 rabbit polyclonal ab. (Cat# AB3560P Millipore), Anti-phosphorylated Trkb rabbit polyclonal antibody. TrkB-Y515 (Cat# ab51187 Abcam, Cambridge, MA, USA), TrkB goat antibody (Cat#GT15080 Neuromics, Edina, MN, USA), GAPDH, mouse monoclonal ab. (Cat# MAB374, Millipore), NR2B mouse monoclonal ab. (Cat# 05-920. Millipore). Blots were then rinsed three times for 10 minutes each with TBS 0.05% Tween 20 and then incubated at room temperature for 1 hour in secondary antibody against the primary antibody host species dissolved in blocking solution. Membranes were again rinsed three times with TBS 0.05% Tween 20. To visualize immunoreactive bands, SuperSignal enhanced chemiluminescent (ECL) western blot detection reagents (Thermo Scientific, Rockford, IL, USA) were utilized along with an imaging system (G-Box, Syngene, Frederick, MD, USA). Densitometric bands were normalized using GAPDH. Densitometric analysis was performed using ImageJ (NIH, Bethesda, MD, USA).

Laser Capture Microscopy

Rats were anesthetized with inactin (100mg/kg i.p.) and decapitated. Brains were isolated and frozen in isopentane cooled on dry ice. Forebrain slices were sectioned through the hypothalamus at 10um-thickness to isolate the SON. Sections were mounted onto PEN membrane-coated slides (Arturus Bioscience, Mountain View, CO, USA). Sections were then

thawed momentarily, then fixed in chilled 100% methanol for three minutes, followed by three washes in cold diethylpyrocarbonate (DEPC)-PBS. Slides were then blocked in DEPC-PBS diluent for five minutes. Incubation in primary guinea pig anti-(Arg^8)-VP (Peninsula Labs, San Carlos, CA. Cat#T-5048) at 1:50 dilution in DEPC-PBS was carried out for five minutes, followed by two washes in DEPC-PBS. Slides were then incubated in secondary $Cy^{TM}3$ conjugated affinipure donkey anti-guinea pig (Jackson Immunorsearch Laboratories, code 706-165-148) for five minutes, entirely covered from ambient light to preserve fluorophore. Three more DEPC-PBS washes followed the secondary incubation.

Labeled SON Cell Capture

An Arcturus Veritas Microdissection instrument, which utilizes the infrared capture laser with an ultraviolet cutting laser, was used to laser capture the AVP-labelled neurons. Neurons that were selected for excision of tissue slice exhibited visible and complete staining of the cytoplasmic compartment. The infrared laser beam was positioned above the brain tissue, which is placed between the PEN membrane slide and the capture cap coated with a thermal plastic. The focused laser beam pulse melted the plastic onto the region of interest, allowing removal of the selected AVP-labelled cells from tissue.

RNA Extraction and Amplification

All conditions were carried out in an RNAse-free environment. The capture cap containing seven to ten neurons was immediately transferred to a 0.5-ml tube containing 30ul of ArrayPure Nano-Scale Lysis Solution with 5.0 g of proteinase K (product # MPS04050; Epicentre Biotechnol Inc. Madison, WI, USA). Total RNA was isolated from the collected AVP

cells using ArrayPure Nano-Scale RNA Purification Kit reagents (Epicentre Biotechnology) as described previously[43]. RNA samples were stored at -80^{o}C. Single cell RNA samples were evaluated using a Nanodrop Spectrophotometer (Nanodrop 2000c Spectrophotometer; Thermo Fisher Scientific Inc., Waltham, MA, USA) to measure the RNA content and identify contamination in the sample. An aliquot of 1–2ul per cellular RNA sample was amplified with TargetAmp 2-Round Aminoallyl-aRNA Amplification Kit materials (Epicentre Biotechnol Inc.).

Quantitative Reverse Transcriptase-Polymerase Chain Reaction (qRt-PCR)

Less than 50 ng of the synthesized aminoallyl-aRNA from laser-microdissected AVP cells was reverse-transcribed to cDNA with Sensiscript RT Kit reagents (product no.205213; Qiagen Inc., Valencia, CA, USA) in accordance with the manufacturer's instructions. A single RT reaction mixture consisted of 2ul of 10 x RT buffer, 2ul of dNTP mix (final concentration: 5uM), 2ul of oligo-dT primer solution (final concentration: 10ul), 1ul of RNase inhibitor (final concentration: 10 U/ul), 1ul of Sensiscript reverse transcriptase solution, and aRNA dissolved in sufficient RNase-free water to yield a total volume of 20ul. Forward and reverse primers for target genes (Table 1) were obtained from Integrated DNA Technologies (Coralville, IA, USA). For PCR, samples consisted of 2ul of cDNA, 8.3 ml of RNase/DNase-free water, 2ul of each primer, and 12.5ul of iQ SYBR Green Supermix (product no. 170-8880; Bio-Rad, Hercules, CA, USA). PCR reactions were performed in a Bio-Rad iQTM5 iCycler system, with the cyclic parameters: initial denaturation at 95^{o}C for 3 min, followed by 50 cycles of 1.1 min each (40 s at 94^{o}C; followed by 30 s at 60^{o}C for TRPV and AVPs and 30 s at 95^{o}C followed by 1 min at 65^{o}C for GAPDH). The housekeeping gene, GAPDH, was used for normalization of mRNA expression. In each real-time RT-PCR analysis, no-template and –RT controls were performed.

For AVP heterogeneous nuclear hnRNA, an additional reaction was also performed in the absence of reverse transcriptase to account for DNA contamination in the sample. Melt curves generated were analyzed to identify nonspecific products and primer-dimers. The data were analyzed by the $2^{-\Delta\Delta C}{}_T$ method as previously described[43]. For calculation of individual $2^{-\Delta\Delta C}{}_T$ value, the individual CT value of housekeeping gene (GAPDH) is subtracted from the corresponding CT value of genes of interest. This value is then subtracted from the difference between the average of the housekeeping and the gene of interest of the control to give the $2^{-\Delta\Delta C}{}_T$ value as previously described[43].

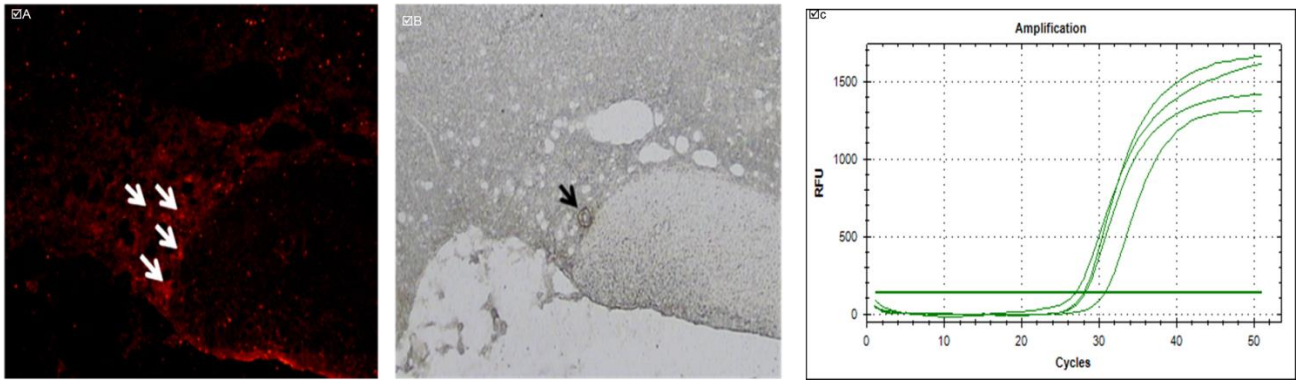

Figure 13. Digital images of AVP MNCs in the SON identified through quick immunostaining (A), neuron dissected by laser capture microscopy captured for later quantitative reverse transcriptase-polymerase chain reaction analysis (B), and an example of an amplification curve showing relative fluorescence (RFU) in (C).

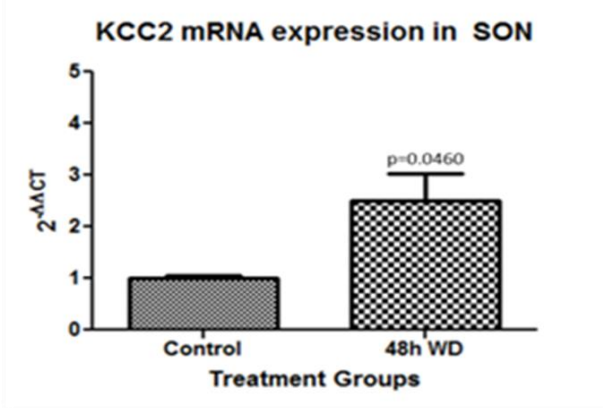

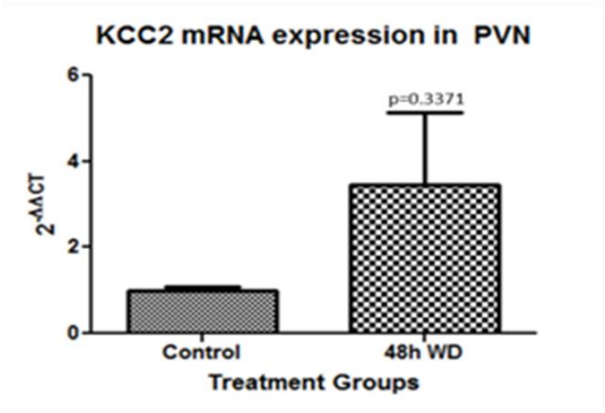

Figure 14. KCC2 mRNA expression in laser-captured AVP SON neurons from control and WD animals. WD significantly increased KCC2 expression in the SON (control, 1.0 ± 0.06 WD 2.5 ± 0.52) *n* = 4.

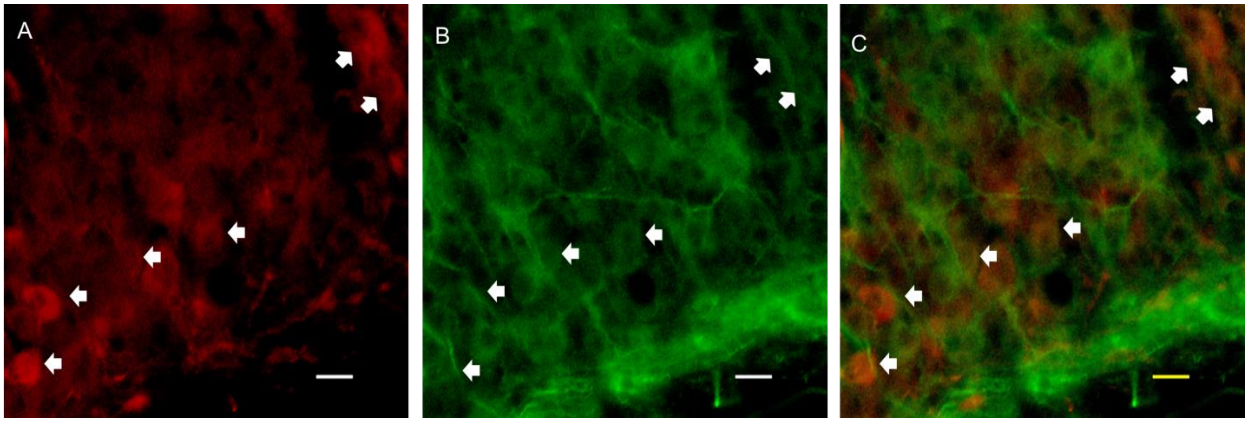

Figure 15. Immunofluorescence of AVP (A) and KCC2 (B) within the SON and a merged digital image (C). Cells labeled with both AVP and KCC2 are indicated with arrows. Scale bar = 20 um.

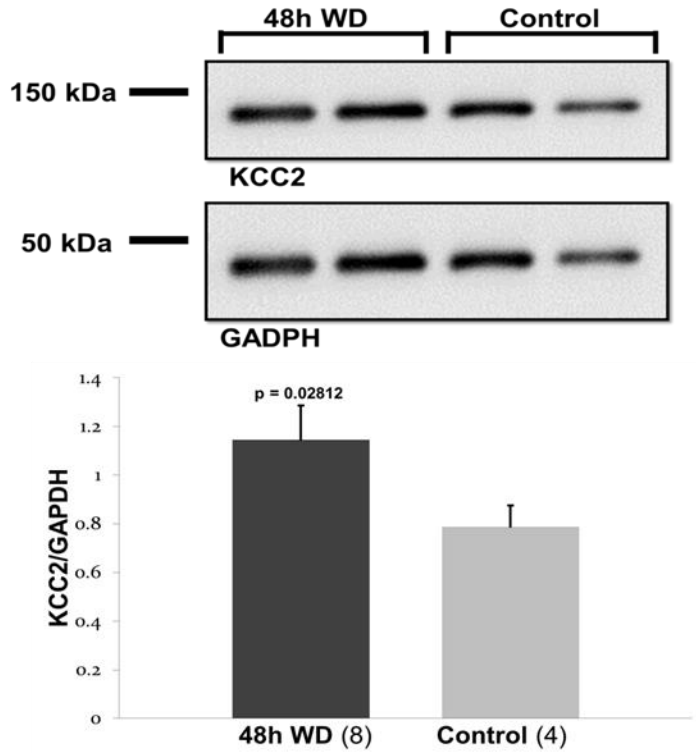

Figure 16. KCC2 protein expression in SON punches from control and WD animals. WD significantly increased KCC2 protein expression in the SON (control n=4, 0.79 + 0.08; WD n=8, 1.15 + 0.14)

References

1. Bourque CW. Central mechanisms of osmosensation and systemic osmoregulation. *Nat Rev Neurosci*. 2008;9(7):519–31. doi:10.1038/nrn2400.

2. Mckinley MJ, Johnson AK. The Physiological Regulation of Thirst and Fluid Intake. 2004:1–6.

3. Scott V, Brown CH. State-dependent plasticity in vasopressin neurones: dehydration-induced changes in activity patterning. *J Neuroendocrinol*. 2010;22(5):343–54. doi:10.1111/j.1365-2826.2010.01961.x.

4. Forsling ML, Montgomery H, Halpin D, Windle RJ, Treacher DF. Daily patterns of secretion of neurohypophysial hormones in man: effect of age. *Exp Physiol*. 1998;83:409–418.

5. Bouley R, Hawthorn G, Russo LM, Lin HY, Ausiello D a, Brown D. Aquaporin 2 (AQP2) and vasopressin type 2 receptor (V2R) endocytosis in kidney epithelial cells: AQP2 is located in "endocytosis-resistant" membrane domains after vasopressin treatment. *Biol Cell*. 2006;98:215–232. doi:10.1042/BC20040054.

6. Bankir L, Bichet DG, Bouby N. Vasopressin V2 receptors, ENaC, and sodium reabsorption: a risk factor for hypertension? *Am J Physiol Renal Physiol*. 2010;299(5):F917–28. doi:10.1152/ajprenal.00413.2010.

7. Nishimoto G, Zelenina M, Li D, et al. Arginine vasopressin stimulates phosphorylation of aquaporin-2 in rat renal tissue. *Am J Physiol*. 1999;276:F254–F259.

8. Byron KL. Vasopressin stimulates Ca2+ spiking activity in A7r5 vascular smooth muscle cells via activation of phospholipase A2. *Circ Res*. 1996;78(5):813–820. doi:10.1161/01.RES.78.5.813.

9. Nemenoff RA. VASOPRESSIN SIGNALING PATHWAYS IN VASCULAR SMOOTH MUSCLE. *Front Biosci*. 1998;3(10). Available at: https://www.bioscience.org/1998/v3/d/nemenoff/nemenoff.pdf.

10. Leng G, Brown CH, Bull PM, et al. Responses of magnocellular neurons to osmotic stimulation involves coactivation of excitatory and inhibitory input: an experimental and theoretical analysis. *J Neurosci*. 2001;21(17):6967–77. Available at: http://www.ncbi.nlm.nih.gov/pubmed/11517284.

11. Schrier RW, Berl T, Anderson RJ. Osmotic and nonosmotic control of vasopressin release. *Am J Physiol - Ren Physiol*. 1979;236(4):F321–F332.

12. Richard D, Bourque CW. Synaptic control of rat supraoptic neurones during osmotic stimulation of the organum vasculosum lamina terminalis in vitro. *J Physiol*. 1995;489 (Pt 2:567–577. doi:10.1159/000126174.

13. Brown CH. Rhythmogenesis in vasopressin cells. *J Neuroendocrinol*. 2004;16(9):727–39. doi:10.1111/j.1365-2826.2004.01227.x.

14. Brown CH, Bourque CW. Mechanisms of rhythmogenesis: insights from hypothalamic vasopressin neurons. *Trends Neurosci*. 2006;29(2):108–15. doi:10.1016/j.tins.2005.11.005.

15. Bourque CW, Oliet SH, Richard D. Osmoreceptors, Osmoreception, and Osmoregulation. 1994. doi:10.1006/frne.1994.1010.

16. Csáki Á, Kocsis K, Kiss J, Halász B. Localization of putative glutamatergic/aspartatergic neurons projecting to the supraoptic nucleus area of the rat hypothalamus. *Eur J Neurosci*. 2002;16(1):55–68. doi:10.1046/j.1460-9568.2002.02059.x.

17. Potapenko ES, Biancardi VC, Zhou Y, Stern JE. Altered astrocyte glutamate transporter regulation of hypothalamic neurosecretory neurons in heart failure rats. *Am J Physiol Regul Integr Comp Physiol*. 2012;303(3):R291–300. doi:10.1152/ajpregu.00056.2012.

18. Fleming TM, Scott V, Naskar K, Joe N, Brown CH, Stern JE. State-dependent changes in astrocyte regulation of extrasynaptic NMDA receptor signalling in neurosecretory neurons. *J Physiol*. 2011;589(Pt 16):3929–41. doi:10.1113/jphysiol.2011.207340.

19. Stern JE, Potapenko ES. Enhanced NMDA receptor-mediated intracellular calcium signaling in magnocellular neurosecretory neurons in heart failure rats. *Am J Physiol Regul Integr Comp Physiol*. 2013;305(4):R414–22. doi:10.1152/ajpregu.00160.2013.

20. Stern JE, Galarreta M, Foehring RC, Hestrin S, Armstrong WE. Differences in the Properties of Ionotropic Glutamate Synaptic Currents in Oxytocin and Vasopressin Neuroendocrine Neurons. *J Neurosci*. 1999;19(9):3367–3375.

21. Boudaba C, Linn DM, Halmos KC, Tasker JG. Increased tonic activation of presynaptic metabotropic glutamate receptors in the rat supraoptic nucleus following chronic dehydration. *J Physiol*. 2003;551(3):815–823. doi:10.1113/jphysiol.2003.042739.

22. Panatier A, Oliet SHR. Neuron-glia interactions in the hypothalamus. *Neuron Glia Biol*. 2006;2(1):51–8. doi:10.1017/S1740925X06000019.

23. Nissen BYR, Cunningham JT, Renaud LEOP. Lateral Hypothalamic Lesions Alter Baroreceptor-Evoked Inhibition of Rat SON VP Neurons. *J Physiol*. 1993;470:751–766.

24. Ohbuchi T, Yokoyama T, Saito T, et al. Brain-derived neurotrophic factor inhibits spontaneous inhibitory postsynaptic currents in the rat supraoptic nucleus. *Brain Res*. 2009;1258:34–42. doi:10.1016/j.brainres.2008.12.057.

25. Matsumoto T, Numakawa T, Yokomaku D, et al. Brain-derived neurotrophic factor-induced potentiation of glutamate and GABA release: different dependency on signaling pathways and neuronal activity. *Mol Cell Neurosci*. 2006;31(1):70–84. doi:10.1016/j.mcn.2005.09.002.

26. Panatier A, Gentles SJ, Bourque CW, Oliet SHR. Activity-dependent synaptic plasticity in the supraoptic nucleus of the rat hypothalamus. *J Physiol*. 2006;573(Pt 3):711–21. doi:10.1113/jphysiol.2006.109447.

27. Pak CW, Currás-Collazo MC. Expression and plasticity of glutamate receptors in the supraoptic nucleus of the hypothalamus. *Microsc Res Tech*. 2002;56(2):92–100. doi:10.1002/jemt.10017.

28. Di S, Tasker JG. Dehydration-induced synaptic plasticity in magnocellular neurons of the hypothalamic supraoptic nucleus. *Endocrinology*. 2004;145(11):5141–9. doi:10.1210/en.2004-0702.

29. Brown CH, Bains JS, Ludwig M, Stern JE. Physiological regulation of magnocellular neurosecretory cell activity: integration of intrinsic, local and afferent mechanisms. *J Neuroendocrinol*. 2013;25(8):678–710. doi:10.1111/jne.12051.

30. Grindstaff RR, Cunningham JT. Cardiovascular regulation of vasopressin neurons in the supraoptic nucleus. *Exp Neurol*. 2001;171(2):219–26. doi:10.1006/exnr.2001.7745.

31. Chakfe Y, Bourque CW. Excitatory peptides and osmotic pressure modulate mechanosensitive cation channels in concert. *Nat Neurosci*. 2000;3(6):572–9. doi:10.1038/75744.

32. Israel J-M, Poulain D a, Oliet SHR. Glutamatergic inputs contribute to phasic activity in vasopressin neurons. *J Neurosci*. 2010;30(4):1221–32. doi:10.1523/JNEUROSCI.2948-09.2010.

33. Potapenko ES, Biancardi VC, Zhou Y, Stern JE. Astrocytes modulate a postsynaptic NMDA-GABAA-receptor crosstalk in hypothalamic neurosecretory neurons. *J Neurosci*. 2013;33(2):631–40. doi:10.1523/JNEUROSCI.3936-12.2013.

34. Choe KY, Olson JE, Bourque CW. Taurine release by astrocytes modulates osmosensitive glycine receptor tone and excitability in the adult supraoptic nucleus. *J Neurosci*. 2012;32(36):12518–27. doi:10.1523/JNEUROSCI.1380-12.2012.

35. Haam J, Popescu IR, Morton L a, et al. GABA is excitatory in adult vasopressinergic neuroendocrine cells. *J Neurosci*. 2012;32(2):572–82. doi:10.1523/JNEUROSCI.3826-11.2012.

36. Li Y, Stern JE. Activation of postsynaptic GABAB receptors modulate the firing activity of supraoptic oxytocin and vasopressin neurones: Role of calcium channels. *J Neuroendocrinol*. 2004;16:119–130. doi:10.1111/j.0953-8194.2004.01148.x.

37. Trudel E, Bourque CW. Central clock excites vasopressin neurons by waking osmosensory afferents during late sleep. *Nat Publ Gr*. 2010;13(4):467–474. doi:10.1038/nn.2503.

38. Ji LL, Fleming T, Penny ML, Toney GM, Cunningham JT. Effects of water deprivation and rehydration on c-Fos and FosB staining in the rat supraoptic nucleus and lamina terminalis region. *Am J Physiol Regul Integr Comp Physiol*. 2005;288(1):R311–R321. doi:10.1152/ajpregu.00399.2004.

39. Goldsmith SR. Current Treatments and Novel Pharmacologic Treatments for Hyponatremia in Congestive Heart Failure. *Am J Cardiol*. 2005;95:14B–23B. doi:10.1016/j.amjcard.2005.03.004.

40. Schrier RW, Niederberger M. Paradoxes of body fluid volume regulation in health and disease. A unifying hypothesis. *West J Med*. 1994;161(4):393–408. Available at: http://www.pubmedcentral.nih.gov/articlerender.fcgi?artid=1022621&tool=pmcentrez&rendertype=abstract.

41. Potapenko ES, Biancardi VC, Florschutz RM, Ryu PD, Stern JE. Inhibitory-excitatory synaptic balance is shifted toward increased excitation in magnocellular neurosecretory cells of heart failure rats. *J Neurophysiol*. 2011;106(3):1545–57. doi:10.1152/jn.00218.2011.

42. Schrier RW. Water and sodium retention in edematous disorders: role of vasopressin and aldosterone. *Am J Med*. 2006;119(7 Suppl 1):S47–53. doi:10.1016/j.amjmed.2006.05.007.

43. Carreño FR, Walch JD, Dutta M, Nedungadi TP, Cunningham JT. Brain-derived neurotrophic factor-tyrosine kinase B pathway mediates NMDA receptor NR2B subunit phosphorylation in the supraoptic nuclei following progressive dehydration. *J Neuroendocrinol*. 2011;23(10):894–905. doi:10.1111/j.1365-2826.2011.02209.x.

44. Currás-Collazo MC, Dao J. Osmotic activation of the hypothalamo-neurohypophysial system reversibly downregulates the NMDA receptor subunit, NR2B, in the supraoptic nucleus of the hypothalamus. *Mol Brain Res*. 1999;70(2):187–196. doi:10.1016/S0169-328X(99)00129-1.

45. Köhr G, Jensen V, Koester HJ, et al. Intracellular domains of NMDA receptor subtypes are determinants for long-term potentiation induction. *J Neurosci*. 2003;23(34):10791–9. Available at: http://www.ncbi.nlm.nih.gov/pubmed/14645471.

46. Choe KY, Han SY, Cunningham JT, et al. High Salt Intake Increases Blood Pressure via BDNF- Mediated Downregulation of KCC2 and Impaired Baroreflex Inhibition of Vasopressin Neurons Article High Salt Intake Increases Blood Pressure via BDNF-Mediated Downregulation of KCC2 and Impaired Barorefle. *Neuron*. 2015:1–12. doi:10.1016/j.neuron.2014.12.048.

47. Aguado F et al. BDNF regulates spontaneous correlated activity at early developmental stages by increasing synaptogenesis and expression of the K+/Cl- co-transporter KCC2. *Development*. 2003;130(7):1267–1280. doi:10.1242/dev.00351.

48. Suen PC, Wu K, Levine ES, et al. Brain-derived neurotrophic factor rapidly enhances phosphorylation of the postsynaptic N-methyl-D-aspartate receptor subunit 1. *Proc Natl Acad Sci U S A*. 1997;94(15):8191–5. Available at: http://www.pubmedcentral.nih.gov/articlerender.fcgi?artid=21579&tool=pmcentrez&rendertype=abstract.

49. Yamada K, Nabeshima T. Current Perspective Brain-Derived Neurotrophic Factor / TrkB Signaling in Memory Processes. *J Pharmocol Sci*. 2003;91:267–270.

50. Arancibia S, Lecomte a, Silhol M, Aliaga E, Tapia-Arancibia L. In vivo brain-derived neurotrophic factor release and tyrosine kinase B receptor expression in the supraoptic nucleus after osmotic stress stimulus in rats. *Neuroscience*. 2007;146(2):864–73. doi:10.1016/j.neuroscience.2007.01.057.

51. Carvalho AL, Caldeira M V, Santos SD, Duarte CB. Role of the brain-derived neurotrophic factor at glutamatergic synapses. *Br J Pharmacol*. 2009;153(S1):S310–S324. doi:10.1038/sj.bjp.0707509.

52. Lobo MK, Covington HE, Chaudhury D, et al. Cell type-specific loss of BDNF signaling mimics optogenetic control of cocaine reward. *Science*. 2010;330(6002):385–90. doi:10.1126/science.1188472.

53. Klau M, Hartmann M, Erdmann KS, Heumann R, Lessmann V. Reduced number of functional glutamatergic synapses in hippocampal neurons overexpressing full-length TrkB receptors. *J Neurosci Res*. 2001;66(3):327–36. Available at: http://www.ncbi.nlm.nih.gov/pubmed/11746350. Accessed April 3, 2015.

54. Caldeira M V, Melo C V, Pereira DB, Carvalho RF, Carvalho AL, Duarte CB. BDNF regulates the expression and traffic of NMDA receptors in cultured hippocampal neurons. *Mol Cell Neurosci*. 2007;35(2):208–19. doi:10.1016/j.mcn.2007.02.019.

55. Huang Y, Ko H, Cheung ZH, et al. Dual actions of brain-derived neurotrophic factor on GABAergic transmission in cerebellar Purkinje neurons. *Exp Neurol*. 2012;233(2):791–8. doi:10.1016/j.expneurol.2011.11.043.

56. Xu F, Plummer MR, Len G-W, et al. Brain-derived neurotrophic factor rapidly increases NMDA receptor channel activity through Fyn-mediated phosphorylation. *Brain Res*. 2006;1121(1):22–34. doi:10.1016/j.brainres.2006.08.129.

57. Wu K, Len G-W, McAuliffe G, et al. Brain-derived neurotrophic factor acutely enhances tyrosine phosphorylation of the AMPA receptor subunit GluR1 via NMDA receptor-dependent mechanisms. *Brain Res Mol Brain Res*. 2004;130(1-2):178–86. doi:10.1016/j.molbrainres.2004.07.019.

58. Kessels HW, Malinow R. Synaptic AMPA receptor plasticity and behavior. *Neuron*. 2009;61(3):340–50. doi:10.1016/j.neuron.2009.01.015.

59. Malinow R. AMPA receptor trafficking and long-term potentiation. *Philos Trans R Soc Lond B Biol Sci*. 2003;358(1432):707–14. doi:10.1098/rstb.2002.1233.

60. Malinow R, Malenka RC. AMPA receptor trafficking and synaptic plasticity. *Annu Rev Neurosci*. 2002;25:103–26. doi:10.1146/annurev.neuro.25.112701.142758.

61. Lincoln D, Wakerley JB. Electrophysiological Evidence for the Activation of Supraoptic Neurones During the Release of Oxytocin. *J Physiol*. 1974;242:533–554.

62. Fitzsimons JT. Angiotensin, thirst, and sodium appetite. *Physiol Rev*. 1998;78(3):583–686. Available at: http://www.ncbi.nlm.nih.gov/pubmed/22913624.

63. Armstrong WE, Smith BN, Tian M. Electrophysiological characteristics of immunochemically identified rat oxytocin and vasopressin neurones in vitro. *J Physiol*. 1994;475(1):115–28. Available at: http://www.pubmedcentral.nih.gov/articlerender.fcgi?artid=1160359&tool=pmcentrez&rendertype=abstract.

64. Tribollet E, Armstrong WE, Dubois-Dauphin M, Dreifuss JJ. Extra-hypothalamic afferent inputs to the supraoptic nucleus area of the rat as determined by retrograde and anterograde tracing techniques. *Neuroscience*. 1985;15(1):135–48. Available at: http://www.ncbi.nlm.nih.gov/pubmed/4010932.

65. Armstrong WE, Smith BN, Tian M. Electrophysiological characteristics of immunochemically identified rat oxytocin and vasopressin neurones in vitro. *J Physiol*. 1994;475(1):115–28. Available at: http://www.pubmedcentral.nih.gov/articlerender.fcgi?artid=1160359&tool=pmcentrez&rendertype=abstract.

66. Verbalis JG, Baldwin EF, Robinson a G. Osmotic regulation of plasma vasopressin and oxytocin after sustained hyponatremia. *Am J Physiol*. 1986;250(3 Pt 2):R444–R451.

67. Sharif Naeini R, Witty M-F, Séguéla P, Bourque CW. An N-terminal variant of Trpv1 channel is required for osmosensory transduction. *Nat Neurosci*. 2006;9(1):93–8. doi:10.1038/nn1614.

68. Paxinos G, Watson C. *The Rat Brain in Stereotaxic Coordinates, Sixth Edition*. Academic Press; 2007. Available at: http://www.amazon.com/Brain-Stereotaxic-Coordinates-Sixth-Edition/dp/0125476124. Accessed August 5, 2013.

69. Ponzio T a, Fields RL, Rashid OM, Salinas YD, Lubelski D, Gainer H. Cell-type specific expression of the vasopressin gene analyzed by AAV mediated gene delivery of promoter deletion constructs into the rat SON in vivo. *PLoS One*. 2012;7(11):e48860. doi:10.1371/journal.pone.0048860.

70. Son SJ, Filosa J a, Potapenko ES, et al. Dendritic peptide release mediates interpopulation crosstalk between neurosecretory and preautonomic networks. *Neuron*. 2013;78(6):1036–49. doi:10.1016/j.neuron.2013.04.025.

71. Bradford MM. A rapid and sensitive method for the quantitation of microgram quantities of protein utilizing the principle of protein-dye binding. *Anal Biochem*. 1976;72(1-2):248–254. doi:10.1016/0003-2697(76)90527-3.